DEVELOPMENT AND APPLICATION OF HIGH-FIELD, HIGH-GRADIENT PULSED FIELD GRADIENT NMR FOR STUDIES OF DIFFUSION BEHAVIOR OF LIPIDS IN MODEL MEMBRANES

By

MONICA DANIELLE SANDERS

A DISSERTATION PRESENTED TO THE GRADUATE SCHOOL
OF THE UNIVERSITY OF FLORIDA IN PARTIAL FULFILLMENT
OF THE REQUIREMENTS FOR THE DEGREE OF
DOCTOR OF PHILOSOPHY

UNIVERSITY OF FLORIDA

2009

To my mother, who has relentlessly encouraged me throughout my life and has taught me the importance of hard work, education and independence

ACKNOWLEDGMENTS

I thank my committee chair, Dr. Sergey Vasenkov, for his constant guidance and support throughout my work, my lab partner, Amrish Menjoge, for his advice and friendship, the staff of the Advanced Magnetic Resonance Imaging and Spectroscopy facility, especially Dr. Dan Plant, for numerous discussions and technical support, and my collaborators which include Konstantin Ulrich for developmental studies, and Robert Mueller and Amrish Menjoge, for Monte Carlo simulation work.

TABLE OF CONTENTS

LIST OF TABLES

LIST OF FIGURES

LIST OF ABBREVIATIONS

AFM	Atomic Force Microscopy
CHOL	Cholesterol
DOPC	1,2-dioleoyl-*sn*-glycero-3-phosphocholine
DPPC	1,2-dipalmitoyl-*sn*-glycero-3-phosphocholine
ESR	Electron Spin Resonance
FCS	Fluorescence Correlation Spectroscopy
FID	Free Induction Decay
FRAP	Fluorescence Recover After Photobleaching
FRET	Fluorescence Resonance Energy Transfer
MAS NMR	Magic Angle Spinning Nuclear Magnetic Resonance
MSD	Mean Square Displacement
NMR	Nuclear Magnetic Resonance
PC	Phosphocholine
PFG NMR	Pulsed-Field Gradient Nuclear Magnetic Resonance
PGSE	PFG NMR Spin Echo Pulse Sequence
STE	PFG NMR Stimulated Echo Pulse Sequence
STE LED	PFG NMR Stimulated Echo Longitudinal Encode-Decode Pulse Sequence
SM	Sphingomyelin
SMT	Single Molecule Tracking
SPT	Single Particle Tracking
$A(g)$	Signal measured as a function of magnetic field gradient amplitude
B_e	The amplitude of the field induced by currents from electrons in orbital clouds
B_{ext}	The amplitude of the applied magnetic field from gradients

B_0	The amplitude of the applied static magnetic field in NMR
B_1	The amplitude of the applied field from a radiofrequency pulse in NMR
c	Concentration
D	Diffusion coefficient
D_{H2O}	Measured diffusion coefficient of water
D_{lit}	Known value of diffusion coefficient of water at room temperature
D^m	Measured diffusion coefficient
D_o	Diffusion coefficient for lipids in liquid-ordered domains
$D_{o,t\to 0}$	Unrestricted diffusion inside liquid-ordered domains
E_a	Energy of activation
g	Magnetic field gradient amplitude
g_{H2O}	Uncalibrated amplitude of gradient
g_{act}	Actual amplitude of gradient applied for H_2O calibration
J	Flux
l	Length of elementary diffusion step
l_d	Liquid-disordered
l_o	Liquid-ordered
L	Dimension of simulation lattice
L_o	Dimension of simulation domain
m	Individual spin magnetization
M_z	Magnetization vector along *z*-axis
M_{xy}	Transverse magnetization (magnetization in *xy*-plane)
p_{bld}	Probability of an elementary diffusion through the domain boundary leading into the liquid-ordered phase

p_{blo}	Probability of an elementary diffusion through the domain boundary leading into the liquid-disordered phase
p_{ld}	Probability of an elementary diffusion step inside the liquid-disordered phase in the x or y direction
p_{lo}	Probability of an elementary diffusion step inside the liquid-ordered domain in the x or y direction
P	Probability density
r	Position of molecule in space
R	Gas constant
R_{lo}	Radius of liquid-ordered domains
t	Time
t_{eff}	Effective diffusion time
T	Temperature
T_m	Miscibility transition temperature
T_1	Spin-lattice NMR relaxation – Longitudinal NMR relaxation
T_2	Spin-spin NMR relaxation – Transverse NMR relaxation
z	Position of a nuclei along the z-axis
α	Domain boundary permeability
β	The angle between the direction of the measured diffusivity and the direction of the lateral diffusion of lipids in the bilayer
γ	The gyromagnetic ratio
γ^*	The relative number of molecules that started their trajectories inside l_o domains and were outside the domains at time, t
δ	Duration of gradient pulse
δ^*	Chemical shift
θ	Angle between lipid dipole moments and direction of B_0 field

τ	Duration between $\pi/2$ and π rf pulses in PFG NMR spin echo sequence
τ_1	Duration between first and second $\pi/2$ rf pulses in PFG NMR stimulated echo sequence
τ_2	Duration between second and third $\pi/2$ rf pulses in PFG NMR stimulated echo sequence
τ^*	Duration of radiofrequency pulse
φ	Magnetization phase
ω	Measured frequency
ω_{ref}	Reference frequency
ω_{opt}	Operation frequency of magnet
ω_0	Larmor frequency
Φ	Tip angle
Ψ	Signal attenuation

Abstract of Dissertation Presented to the Graduate School
of the University of Florida in Partial Fulfillment of the
Requirements for the Degree of Doctor of Philosophy

DEVELOPMEMT AND APPLICATION OF HIGH-FIELD, HIGH-GRADIENT PFG NMR STUDIES OF LIPID SELF-DIFFUSION IN PLANAR-SUPPRTED LIPID BILAYERS

By

Monica Danielle Sanders

December 2009

Chair: Sergey Vasenkov
Major: Chemical Engineering

This work presents the development and application of a high-field, high-gradient pulsed field gradient nuclear magnetic resonance technique for studies of lipid lateral diffusion in planar-supported lipid bilayers composed of ternary mixtures of lipids intended to mimic the composition of eukaryotic cell membranes. Lipid rafts are small functional domains that exist in cell membranes. It is widely accepted that rafts participate in many cellular activities such as signal transduction. Lipid rafts in non-activated cells are believed to be smaller than around 200 nm in size and quite unstable. Liquid-ordered domains in model membranes share similar characteristics to lipid rafts. In these studies, domains as large as 10 μm have been observed under certain conditions. However, recent data indicates that much smaller domains can also form and remain stable in these model membranes under certain conditions. In order to accurately characterize lateral transport of lipids in domain-forming model membranes and possibly extract information relevant to the study of lipid rafts, an experimental technique is required which has sufficient spatial resolution and does not disturb the membrane or any liquid-ordered domains which might exist. Pulsed field gradient nuclear magnetic resonance (PFG NMR) allows for the direct observation of molecular

mean square displacements and their related diffusion coefficients in a manner which does not perturb the membrane since additives, such as fluorescently-labeled lipids, are unnecessary. In this work, the use of a high magnetic field strength (17.6 T) coupled with high magnetic field gradient strength of up to 30 T/m affords the use of smaller diffusion times under the conditions of the narrow-pulse approximation which allows for distortion-free monitoring of time-dependent and displacement-dependent diffusion behavior of lipids with superior signal-to-noise. Diffusion measurements conducted on membranes consisting of a mixture of DOPC, SM, and Chol show diffusion behavior which was independent of diffusion time, consistent with the presence of large liquid-ordered domains. Formation of smaller domains was observed in membranes consisting of DOPC, DPPC, and Chol near the miscibility transition temperature which manifests as time-dependent diffusion behavior of lipids. It was verified that this behavior was a consequence of lipid exchange between liquid-ordered domains and the surrounding liquid-disordered environment rather than an NMR relaxation effect. Dynamic Monte Carlo simulations were used in conjunction with time-dependent diffusion results to extract information about domain size and the permeability of the domain boundary. This is the first observation of time-dependent diffusion and estimation of such properties for lipid membranes of any composition.

CHAPTER 1
INTRODUCTION

Lipid Raft Model: Motivation for this Work

A Brief History of the Lipid Raft Hypothesis

Biological membranes of eukaryotic cells are complex systems which cannot be described as structurally homogeneous over a broad range of lengths scales ranging from nanometers to microns. Understanding the structural heterogeneity is crucial to attaining a more fundamental understanding of the role of membrane composition and organization in many important cellular events. Lateral organization of biological membranes has been attracting an increasing amount of attention in the scientific community since the introduction of the fluid mosaic model in the early 1970's.[1] This model, developed by Singer and Nicolson, describes the lipid bilayer of the cell membrane as a neutral two-dimensional solvent that serves as an effective barrier for molecular exchange but does not influence membrane protein function.[2] Singer and Nicholson's work explains the connection between free energy requirements and lipid-protein orientation by showing how membrane molecules orient themselves into bilayers so that hydrophobic and hydrophilic interactions are maximized in order to minimize the free energy state of the system.[1] The fluid mosaic model suggests a random distribution of proteins and lipids in the membrane. (See Figure 1-1) Shortly after this model was published, evidence was presented indicating the presence of "clusters of lipids" in membranes.[3] From then on, the focus on the organization of the lipid components in membranes grew. Over the past decade, our understanding of lipid membrane organization has been further enhanced by the proposal of the lipid raft hypothesis.[4] This hypothesis postulates the existence of small, functional domains in

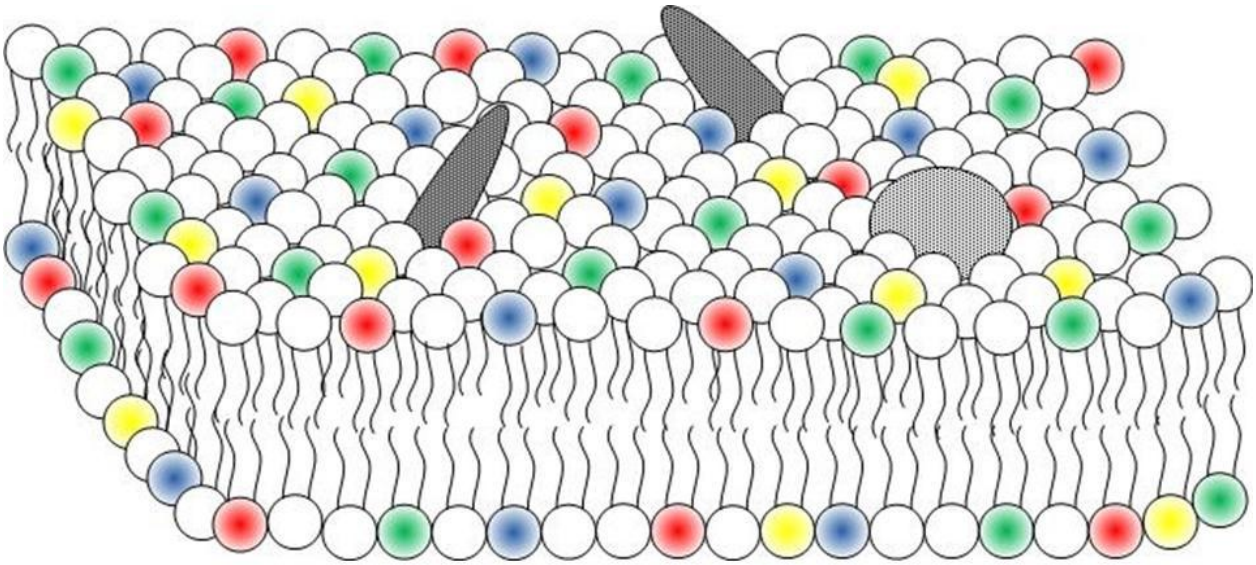

Figure 1-1. Schematic of a lipid bilayer as described by the Fluid Mosaic Model.[1] Colored molecules are intended to represent the random distribution of different types of lipids as originally postulated in this model. Grey molecules represent the proteins associated with the membrane which were also believed to be randomly distributed in the bilayer.

membranes of eukaryotic cell with unique lipid and protein compositions. This paradigm arose from studies of polarized epithelial cells which examined the selective delivery of lipids to the apical and basolateral surfaces of these cells.[5] Early studies concluded that the two leaflets of the cell membrane are different in terms of composition and this difference originates in the Golgi complex where lipids are sorted and clustered before delivery to their destination. They also proposed that membrane proteins are included in these clusters and are transported together with the lipids via transport vesicles.[5]

The lipid raft hypothesis postulates that on the surface of cell membranes, particular clusters organize into domains know as lipid rafts. It has been suggested that lipid rafts serve as platforms that play a role in many cellular functions such as signal transduction.[2] It is also widely hypothesized that lipid rafts play a role in the survival of cancer cells and the ability of viruses to penetrate cell membranes.[6-11] Changes in

membrane composition leading to modifications of the raft properties have been explored as an attractive new strategy to fight lipid raft-related cancer and viral diseases.[12] The success of this approach would be enhanced by detailed knowledge of the structural and dynamic properties of lipid rafts.

Detection in Model Membranes

Studies preformed for the purpose of characterizing the organization and dynamic properties of lipids in biological membranes are conducted both *in vivo* and using synthesized model membranes. *In vivo* studies are complicated by the sheer complexity of the cell membrane. Studies using model membranes can provide a fundamental understanding of intrinsic cell membrane properties by observing characteristic structure, dynamics and organization in less complex, multi-component lipid bilayers. The lipid raft hypothesis suggests a close link[13,14] between lipid rafts and the liquid-ordered (l_o) phase,[15] which can be easily observed in cholesterol- and sphingolipid-rich model membranes.[13,16-19] (see Figure 1-2) For these model membranes, the l_o phase is observed at temperatures above a melting point transition temperature, *viz.* the temperature at which there is a change in the physical state of the lipids from a gel to liquid crystalline fluid phase. Liquid crystalline phases are differentiated into two states (or phases): liquid-disordered and liquid-ordered. The liquid-disordered (l_d) phase is characterized as having an abundance of lipids with the hydrocarbon chains that are mobile and head groups that are hydrated. The bilayer in the l_d state is thinner and less dense when compared to that in the gel state[20] and order parameters for the fatty acid chains are typically > 0.25. Liquid-ordered phases have a higher lipid density resulting in a stiffening of the hydrocarbon chains[21] as characterized by a thicker membrane and significantly higher order parameter. The l_o phase is rich in

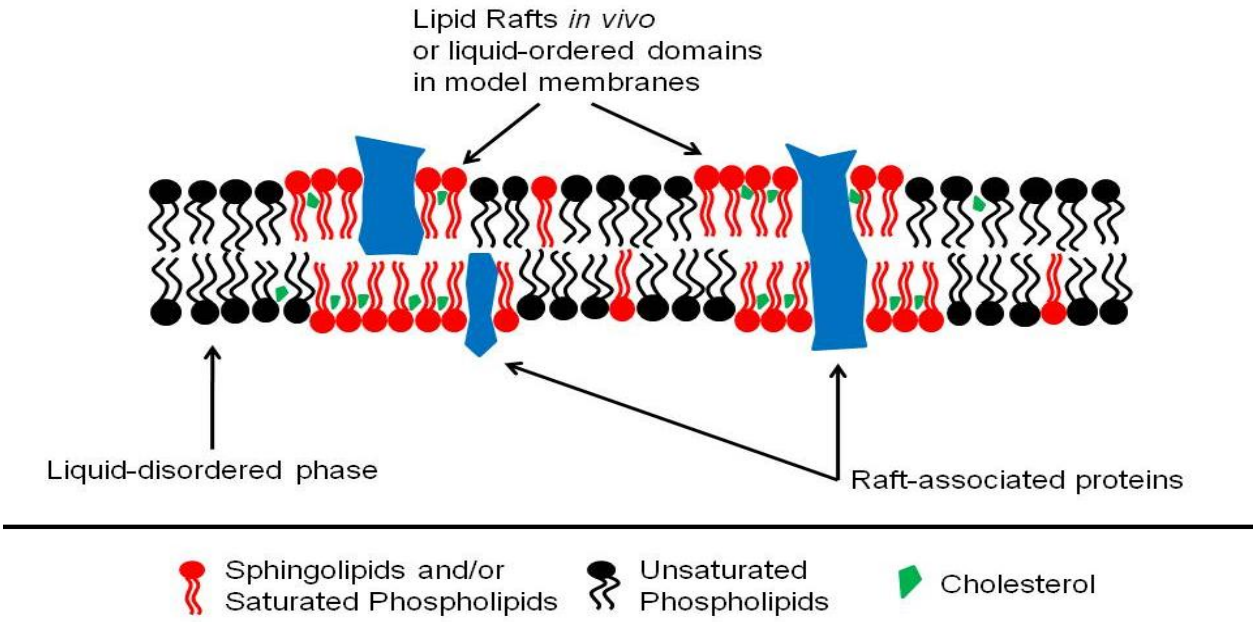

Figure 1-2. Schematic of a lipid bilayer as defined by the lipid raft hypothesis[4] showing the existence of highly ordered domains enriched in certain lipids and cholesterol. The domains in this figure represent lipid rafts in the cell membrane and/or liquid-ordered domains in model membranes. The domains are hypothesized to play key roles any many cellular activities.

sphingolipids and cholesterol in comparison to the l_d phase. For sterol-free membranes, experimental data indicate that only the l_d and gel phases can coexist. Addition of cholesterol can lead to the formation of domains, which exhibit a distinct l_o phase.[15] Since lipid mixtures consisting of unsaturated and saturated phospholipids, sphingolipids and cholesterol can spontaneously form bilayers with clear domain separation under suitable conditions, they have been considered to be suitable model membranes to characterize the lipid organization and properties in cell membranes.[22,23] The development of these model membranes will be discussed further in Chapter 2.

The observation of coexisting l_o and l_d liquid crystalline phases in synthetic lipid mixtures has triggered a number of very detailed investigations regarding the properties of liquid-ordered domains in model membranes by various experimental techniques.

Many initial studies focused on detecting inhomogeneous lipid distribution, characterizing phase transitions, and determining compositional effects in lipid mixtures. The most well-known techniques suitable for such studies are fluorescence microscopy-based techniques such as fluorescence quenching and fluorescence resonance energy transfer (FRET).[17,24-27] Fluorescence-based techniques rely on the excitation of a fluorescently-tagged lipid to show the position and/or the distribution of membrane species of interest. These techniques have been used to investigate the role of cholesterol and other sterols in domain formation, to detect inhomogeneities in ternary mixtures of cholesterol, sphingolipid, and phosphocholine (PC), to generate phase diagrams for common ternary mixtures at physiologically relevant temperatures,[28-31] and to determine partition coefficients of fluorescent probes in l_o and l_d phases.[32,33] Other useful techniques include atomic force microscopy (AFM)[34-37], differential scanning calorimetry[38-40], and various nuclear magnetic resonance (NMR) and electron spin resonance (ESR) techniques.[41-46] Many of the studies detecting domains in model membranes indicate that these domains are very large (> 1 micron) and very stable.[47]

Sizes of Model Rafts *vs.* Lipid Rafts *in vivo*

There have been some questions raised about the discrepancy between the size of domains traditionally observed in model membranes and lipid rafts in cell membranes. Initially, lipid rafts were observed and characterized by detergent extraction of intact cell. Lipids rafts are resistant to solubilization in non-ionic detergents such as Triton X-100 at low temperatures (4°C). Detergent extraction studies showed that certain proteins could partition into these domains as well. Lipid rafts were initially believed to be as large as 500 nm and stable based on detergent extraction experiments.[48] In contrast, more recent experimental evidence suggests that in many

cases only very small (< 200 nm), highly dynamic, and possibly unstable rafts can form in non-activated cells.[3,49-52] Some researchers have expressed doubts about even the existence of lipid rafts as functional entities.[53-55] At the same time, experimental evidence which supports the existence of such domains *in vivo* keeps accumulating.[56-63] It is also believed that small rafts can agglomerate and form larger platforms due to interactions between raft constituents (proteins and lipids).[20,52,64-67] With recent evidence that lipid raft sizes are smaller than l_o domains in model membranes increasing, concerns as to the accuracy of representation by model membranes have been expressed. These concerns do not directly refute the existence of lipid rafts in cells, but rather impress the importance of using caution when extending the results obtained with model membranes to lipid rafts *in vivo*. Recent studies have observed l_o domains on the order of 100 nm in model membranes using FRET,[24,25] AFM,[34,36,68] and solid-state NMR.[43,45,46] These domains are consistently observed at physiological temperatures even when the same membrane system appears to be homogeneous by other methods.[26] The size of the domains observed has been demonstrated to vary as both a function of temperature and composition.[43,69] As the temperature of the raft-containing bilayer is increased to approach the miscibility transition temperature of the lipid mixture, T_m, large micron-sized domains are replaced by smaller domains. Critical fluctuations on the length scale of <50 nanometers are expected when the system is very near T_m.[69] These fluctuations represent the formation and collapse of complexes consisting for the most part of a small number of cholesterol molecules and saturated lipids.[70] It has been suggested that critical fluctuations can be viewed as the onset of domain formation,[71] which is due to the affinity of cholesterol for and dynamic

relationship with saturated lipids.[72-74] While, the study of raft-like domains in model membranes and their relationship to the formation and function of lipid rafts in cell membranes is ongoing, it is quite clear that exchange of lipids between rafts and their surroundings plays a key role in raft formation.

With the focus shifting to much smaller length scales and the role of critical fluctuations in domain formation, it is necessary to employ experimental techniques appropriate for the detection of diffusion dynamics on submicrometer length scales. First, many fluorescence-based techniques, which require attaching labels to lipid molecules, may be inappropriate for studies of structure and dynamics. It has been reported that fluorescent labels can affect the physical properties of small biomolecules, such as lipids, in membranes.[75] Microscopy-based techniques are limited by the optical diffraction limit with the smallest observable length scale for these techniques is often much larger than the predicted size of domains. Methods such as single particle (molecule) tracking as well as improved fluorescence correlation spectroscopy (FCS) methods which allow the resolution to go beyond the optical diffraction limit provide better spatial resolution[34,36,76,77] but are still limited by the requirement of labels. To understand organization in these complex, sensitive systems, it is imperative to utilize an experimental technique with sufficient spatial resolution which will not perturb the membrane organization. NMR spectroscopy offers an attractive alternative to techniques which require labels and underpins the studies in this work.

Studies of Lateral Diffusion in Biologically-Relevant Systems

The dynamics of lipids in biological and model membranes can be significantly affected by the presence of domains. Studies of lipid dynamics can give useful information about domain formation and structure as well as about the domain stability.

Of particular interest to this work, studies of lipid dynamics in domain-forming membranes can give important information about molecular exchange between domains and their surroundings. Characterizing this lipid exchange can lead to a better understanding of lipid lateral dynamics and the structural properties of lipid rafts in cell membrane. Lateral diffusion is expected to play an important role in many membrane processes. In particular, the rate of reaction between ligands (signaling molecules) and receptors might be controlled by lateral diffusion since these intermolecular events are often diffusion-limited. The following section discusses the theoretical treatment of diffusion in lipid membrane focusing on the fundamental of lateral self-diffusion in detail.

The fluid-like properties of lipid bilayers are consequences of lipid mobility within the bilayer. Mobility in this case can be characterized by the two main modes of motion: changes in configuration via vibrational and rotational motions of molecules within the bilayer, and translational motion, which describes the lateral mobility of molecules.[47] It is also possible for lipid molecules to exchange between the two leaflets of the bilayers (lipid flip-flop). This movement, however, is very infrequent having a much longer timescale than studies in this work. These types of motions can be observed via longer timescale techniques to study the interaction and relationship between the two leaflets of the bilayer. However, the particular interest of this work is the manner in which lateral organization of lipids in biological membranes affects translational dynamics (*i.e.*, diffusion).

Diffusion results from the process of stochastic thermal motion of the molecules and can be described by two basic modes: transport diffusion and self-diffusion. (see Figure 1-3) Transport diffusion involves the movement of molecules in order to reduce

macroscopic concentration gradients (or gradients of chemical potential) while self-diffusion occurs in the absence of macroscopic concentration (or chemical potential) gradients. The transport diffusion coefficient describes the relationship between the flux of molecules and a concentration or chemical potential gradient under non-equilibrium conditions. In self-diffusion, molecular transport is characterized by the random translational motion of molecules driven by thermal energy. Self-diffusion occurs in liquid-like systems such as lipid bilayers in the absence of a macroscopic gradient of chemical potential. Self-diffusion can be described and treated similarly to transport diffusion if one considers an uneven

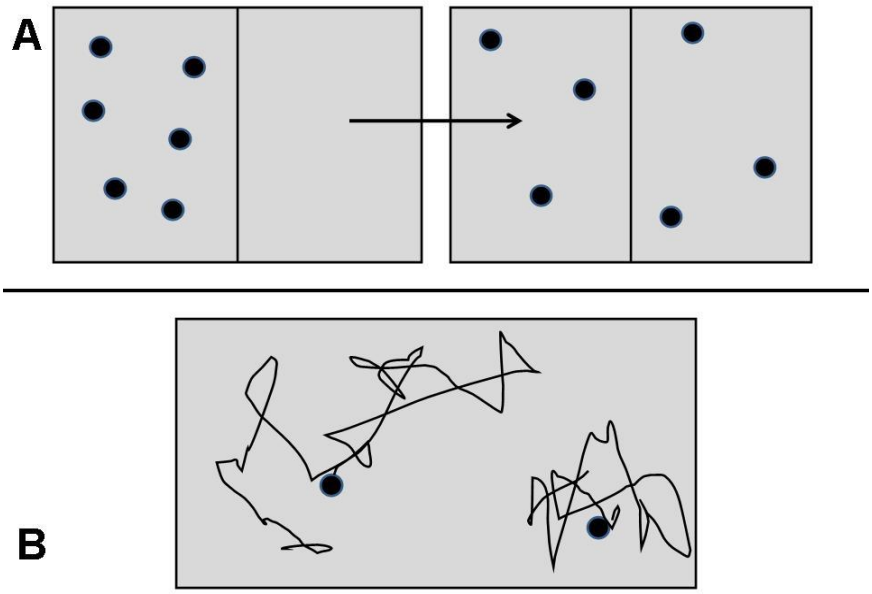

Figure 1-3. Schematic depicting two types of diffusion. A) transport diffusion under circumstances of a concentration gradient and B) self-diffusion in the absence of a macroscopic concentration gradient.

distribution of labeled and unlabeled molecules under conditions when overall molecular concentration remains the same at each point of the considered volume. Many experimental techniques suitable for studies of self-diffusion involve the observation of

labeled molecules in a sea of unlabeled but otherwise identical molecules. In these cases, the self-diffusion coefficient can be derived from the Fick's First Law considering a concentration gradient of labeled molecules. The diffusive flux of labeled molecules is

$$J(r,t) = -D\nabla c(r,t) \qquad (1)$$

where *D* is the self-diffusion coefficient, *r* is the position in space, *t* is the time and $c(r,t)$ is the concentration of (labeled) molecules moving in one-, two-, or three-dimensional space. By applying the principle of conservation of mass, the change in concentration with time at a certain position in space can be described as

$$\frac{\partial c(r,t)}{\partial t} = -\nabla \cdot J(r,t) \qquad (2)$$

The combination of Eq.'s (1) and (2) give Fick's Second Law,

$$\frac{\partial c(r,t)}{\partial t} = \nabla \cdot (D\nabla c(r,t)) \qquad (3)$$

Thermal stochastic motion of molecules will cause the concentration gradient to approach the zero value with increasing diffusion time. The self-diffusion (*D*) in Eq. 3 can be placed before the first gradient operator because this diffusivity is expected to be independent of position (since overall molecular concentration remains the same for all positions). Eq. 3 can be solved by replacing the spatially-dependent concentration term with a term describing the probability that a molecule will diffuse from its initial position r_0 to the position r after time *t*. The solution gives a Gaussian distribution that is also known as diffusion propagator.

$$P(r_0, r, t) = (4\pi Dt)^{-3/2} exp\left\{ -\frac{(r - r_0)^2}{4Dt} \right\} \quad (4)$$

where $P(r_0, r, t)$ is the probability that a molecule with an initial position, r_0, will migrate to a final position, r, after time t. This probability function is a function of the displacement (r-r_0) rather than the initial position. The Einstein relation can be easily derived from the diffusion propagator (Eq. 4). For two-dimensional self-diffusion in a plane such as the surface of the membrane bilayer this relation can be written as

$$\left\langle r^2 \right\rangle = 4Dt \quad (5)$$

where $< r^2 >$ is the mean square displacement (MSD).[78]

In a homogeneous system where molecules diffuse in an unrestricted manner, the description above serves to give the true diffusion coefficient that describes the translational dynamics of the system. In this case, the diffusion coefficient is independent of the time that molecules are given to diffuse (observation time) and so the mean-square displacement of molecules scales linearly with time.[79] Heterogeneous systems incorporate a complication related to the possibility of restriction of free diffusion due to the presences of obstacles. For the case of lipid bilayers, this corresponds to a situation where domains are present in the bilayer. In cases of restricted or partially-restricted diffusion inside of domains it is expected that the propagator will deviate from the Gaussian function. The effective diffusion coefficient as defined by Eq. 5 then becomes dependent on the observation time and the MSD no longer scales linearly with time. At sufficiently short observations times (*i.e.*, corresponding to displacements much smaller than the size of the domain), the diffusion coefficient should be unaffected by any restrictive domain boundaries. At moderate to

large observation times, the molecule is allowed to reach the boundaries of the domain which affect their overall mean-square displacement and measured diffusion coefficient. Results showing time-dependent dynamics can give information about the size of domains as well as the extent of exchange of molecules between these domains and their surroundings and the related permeability of the domain boundaries.

Experimental techniques capable of measuring translational dynamics of lipids in membranes include fluorescence recovery after photobleaching (FRAP)[80-82], fluorescence correlation spectroscopy (FCS)[19,31,83], single particle (molecular) tracking[84-86] and pulsed-field gradient NMR.[87-89] In addition to the properties discussed earlier, lipids in the l_o domains exhibit lower mobility in comparison with the surrounding l_d phase. As mentioned previously, the focus of membrane research is shifting to much smaller length scales due to accumulating evidence of the existence of nano-sized domains both *in vivo* and in model membranes. In the presence of domains, membrane molecules such as lipids or proteins exhibit differences in diffusivities due to restricted diffusion and/or variations in local membrane properties such as molecular packing density. It is very important to utilize experimental techniques that can give information about dynamics over relevant length scales without altering the structural and dynamic properties of the membranes. With current attention focusing on conditions of bilayers very near the miscibility transition temperature, the length scales of interest are much smaller than the sizes of giant l_o domains (around 10 microns) observed in model membranes. As mentioned before, fluorescence microscopy-based techniques are often limited by spatial resolution due to the optical diffraction but are also limited by the requirement for labels. Methods such as single particle (molecule) tracking and atomic

force microscopy as well as improved FCS methods which allow the resolution to go beyond the optical diffraction limit provide better spatial resolution[34,36,68,76,77] but are still limited by the requirement of labels. Nuclear magnetic resonance spectroscopy offers an attractive alternative to experimental techniques that require the attachment of labels. NMR techniques such as magic angle spinning (MAS) NMR and pulsed-field gradient (PFG) NMR spectroscopy as well as a combination of these two techniques (MAS PFG NMR) are used to detect membrane domains and/or study dynamics without perturbing the system with bulky labels. Current PFG NMR techniques to study diffusion are still, however, limited by spatial resolution. The spatial resolution of PFG NMR measurements is mostly determined by the strength of the magnetic field gradients. Recently-used PFG NMR methods employ magnetic field gradients that correspond to spatial resolution comparable to that of some of the microscopy-based techniques. The spatial resolution in these cases is not adequate for direct studies of nano-sized domains. Current experimental techniques have contributed to the understanding of the structure and organization of biomembranes, however they are still unable to fulfill the requirements of sufficient spatial resolution without perturbing environments.

Description of Project

This work describes the development and application of a high-field, high-gradient strength PFG NMR technique used to monitor lateral diffusion of lipids in planar-supported membrane systems. The technological novelty of this work is related to achieving the spatial and temporal resolutions which are superior to those reported in previous PFG NMR studies of lipid membranes under the conditions when sufficiently large NMR signal of lipids can be easily recorded. The advantage of high-field

measurements is directly related to improved signal-to-noise. Application of stronger gradients allows for the use of smaller diffusion times under the conditions of the narrow-pulse approximation which allows for distortion-free monitoring of time-dependent and displacement-dependent diffusion behavior. Until now, the maximum strength of magnetic field gradients, which were applied in PFG NMR studies of lateral diffusion in lipid membranes, was in the range of just several teslas per meter.[87,90] In some special cases, a maximum gradient strength of around 10 T/m was reached.[91] The maximum strength of magnetic field gradients applied in this work is 30 T/m. With the current experimental setup, it is possible to measure the displacement of lipids over length scales relevant to the size of lipid rafts. The temporal resolution of PFG NMR measurements reported in this work are determined by the actual diffusion time used in a pulse sequence rather than the total time required to measure a single diffusivity. The former time intervals can be as small as 5 ms, while the latter can be greater than 1 hour. Results obtained by PFG NMR represent averages of numerous scans to produce data with satisfactory signal-to-noise ratios. A clear requirement for this type of study is that systems remain at steady-state conditions during the measurements; this requirement was always fulfilled for the studies reported in the present work. Simple estimates show that application of such strong field and gradient strengths would increase the temporal and spatial resolutions of diffusion measurements to the extent that diffusion on length scales comparable with size of rafts (< 200 nm) can be directly measured. This was confirmed by the experimental results discussed below. The description of technological development in this work demonstrates that it is now feasible to employ high-field, high-gradient PFG NMR for diffusion studies in planar-

supported lipid membranes. Furthermore, the technique presents advantages over current methods in offering new details about lipid dynamics.

Improvement in the spatial and temporal resolution of lipid diffusion measurements is important due to the following considerations. Detailed information on the influence of membrane inhomogeneities on translational dynamics of lipids in lipid membranes can be obtained only when probing diffusion for displacements comparable to the size of these inhomogeneities. For the limiting case of large displacements and diffusion time, most of the information will be lost due to the averaging over the length scales much larger than the size of membrane inhomogeneities. In addition to a sufficiently high spatial resolution, it is also important to have the ability of monitoring diffusion over a broad range of the mean square displacements (i.e., diffusion times). For molecular displacements comparable with the size of the inhomogeneities, the effective lateral diffusivities of lipids are expected to be dependent on diffusion time. Detailed knowledge of this time-dependent diffusion is crucial to understanding the structure-dynamics relationship in lipid membranes, *i.e.* molecular exchange of lipid molecules. In this work, new details of molecular exchange between domains and their surroundings as well as permeability of the domain boundaries are extracted from the time-dependent diffusion behavior.

Description of the Pulsed-Field Gradient NMR Method

A Brief Overview of Nuclear Magnetic Resonance

Nuclear magnetic resonance spectroscopy is a technique that exploits the inherent magnetic properties of certain atomic nuclei in order to obtain detailed information about the structure and dynamics of molecules. In the framework of classical theory, NMR spectroscopy can be understood by first considering that certain nuclei posses an

intrinsic source of angular momentum known as nuclear spin angular momentum. For a macroscopic system consisting of many nuclei, the total angular momentum is a vector that represents the direction and magnitude of the sum of individual spin angular momenta. Nuclei with non-zero spin angular momentum also have an intrinsic magnetic moment. In a macroscopic system, alignment of magnetic spins of individual nuclei along the direction of the external magnetic field leads to a non-zero net magnetization. (Figure 1-4A) The static magnetic field B_0 exerts a torque on the net magnetization which causes a precessive motion about the direction of the external magnetic field at a frequency know as the Larmor frequency,

$$\omega_0 = -\gamma B_0 \tag{6}$$

where γ is the gyromagnetic ratio of the nucleus under observation and B_0 is the amplitude of the static magnetic field (Figure 1-4B). In NMR, the direction of the B_0 field is usually assumed to coincide with the *z*-axis of the laboratory (*viz*. non-rotating) coordinate system. Magnetic resonance can be achieved by applying an additional magnetic field B_1 that oscillates in the transverse (*x,y*) plane with the Larmor frequency. In NMR spectrometers, the application of a current through the rf coil at the Larmor frequency will rotate the net magnetization vector from the direction of the external magnetic field (*z*-axis) to the transverse plane (Figure 1-4C). The angle that the magnetization is rotated, or the tip angle, is give by

$$\Phi = \gamma B_1 \tau^* \tag{7}$$

where Φ is the tip angle and τ^* is the duration of the rf pulse or B_1 field. A tip angle of 90º will tip the net magnetization vector completely in the transverse *xy*-plane, where the signal is detected. Detection will be discussed in detail later in this section.

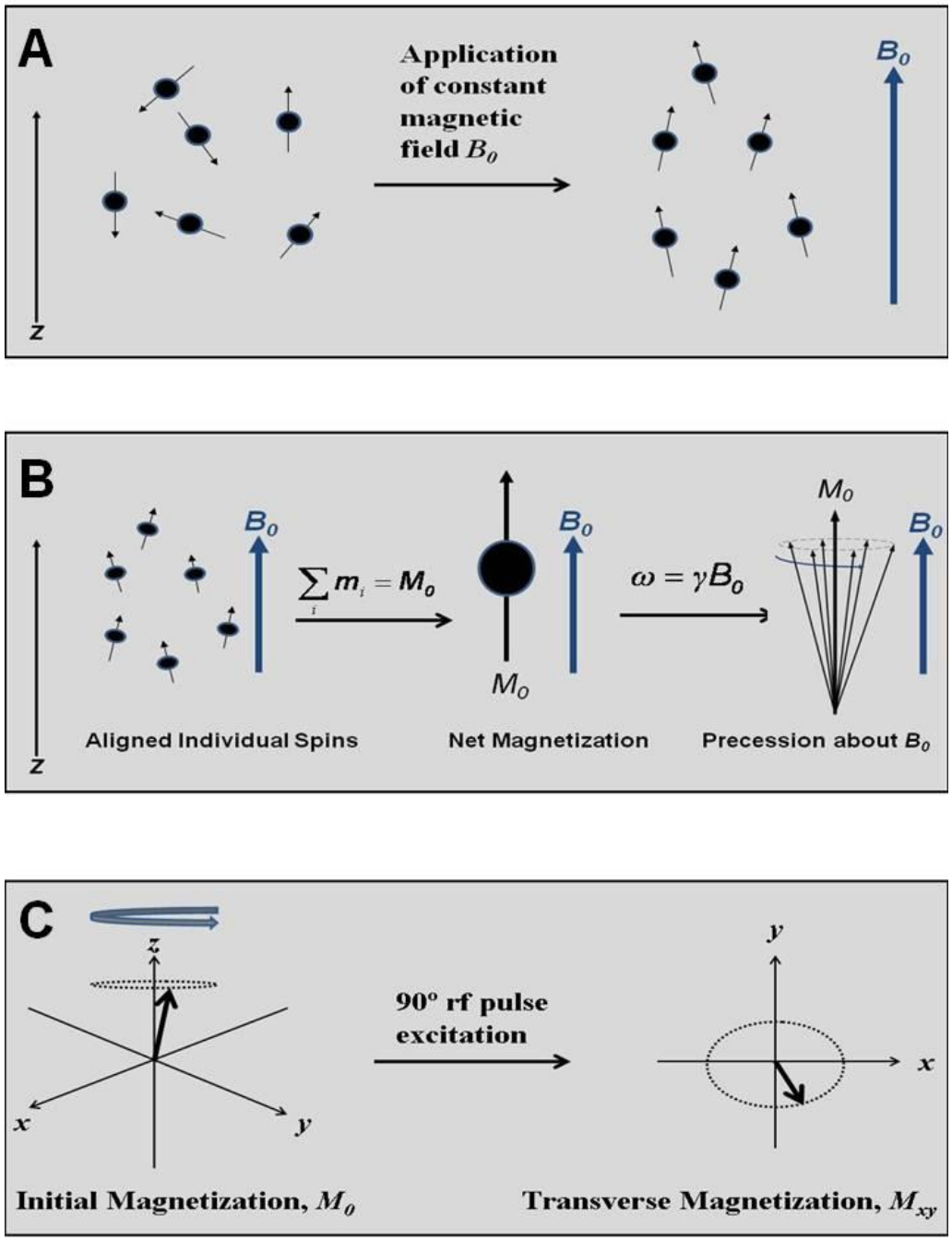

Figure 1-4. Schematic representations of magnetization. A) Alignment of individual magnetic moments in the presence of a static magnetic field. (B) The summation of individual magnetic moments to get a net magnetization and precession in the presence of a static magnetic field. (C) The excitation of a net magnetization vector precessing around the z-axis by a $\pi/2$ radiofrequency pulse to create transverse magnetization.

The excitation of magnetization by a transverse rf pulse guides the system into a non-equilibrium state. The process by which the excited net magnetization vector returns to its equilibrium position with time is known as NMR relaxation. There are two NMR relaxation mechanisms: spin-lattice or longitudinal (T_1) relaxation and spin-spin or transverse (T_2) relaxation. At equilibrium (*i.e.* before the rf pulse), the time-average of the magnetization vector is oriented along the *z*-direction while the transverse magnetization (magnetization in the *xy*-plane) is zero. In a simple approximation spin-lattice relaxation can be viewed as the process by which energy gained from the applied rf pulse is transferred from the excited nucleus (spin) to its surroundings (the lattice) in order to reach thermal equilibrium. This causes the *z*-magnetization to return to its equilibrium value. T_1 relaxation can be described by

$$M_z(t) = M_0\left(1 - e^{-t/T_1}\right) \tag{8}$$

where $M_z(t)$ describes the magnetization in the *z*-axis as a function of time, t, M_0 is the equilibrium magnetization value in the *z*-direction and T_1 is the spin-lattice relaxation time. Spin-lattice relaxation times depend on a number of macroscopic parameters including the strength of the B_0 field and temperature. Spin-spin relaxation is the process that is related to the interactions between the nuclei (spins) themselves. Energy is exchanged between the spins which induce slight changes in their individual local magnetic fields causing a slight change in frequency. Immediately after excitation by the rf pulse, all spins are in phase coherence with each other (*i.e.*, they precess exactly at the same frequency and the accumulated phase is 0). After some time when T_2 relaxation effects are significant, the spins lose coherence, which is reflected by the existence of phase differences for different nuclei. As a result, the transverse

magnetization decays. T_2 NMR relaxation can be described by

$$M_{xy}(t) = M_{xy,0} e^{-t/T_2} \tag{9}$$

where $M_{xy}(t)$ is the transverse magnetization in time, $M_{xy,0}$ is the initial transverse magnetization after excitation, and T_2 is the spin-spin relaxation time. This magnetization eventually decays to its equilibrium value of zero because of T_2 relaxation.

As mention briefly above, the frequency of the signal is detected in the transverse plane. Immediately after the magnetization tipped into the transverse plane by the rf pulse, the signal starts to decay due to T_2. The decaying transverse magnetization that is recorded is referred to as a free induction decay (FID) which is converted from time domain signal to frequency domain signal using Fourier transformation (Figure 1-5). The frequency of signal that is detected varies somewhat from the Larmor frequency. These slight variations are due to a phenomenon known as chemical shift. Electrons in orbital clouds exert currents which produce magnetic fields (B_e). The existence of this additional field leads to a slight deviation of the local magnetic field from the B_0 field. Nuclei with different local environments will experience

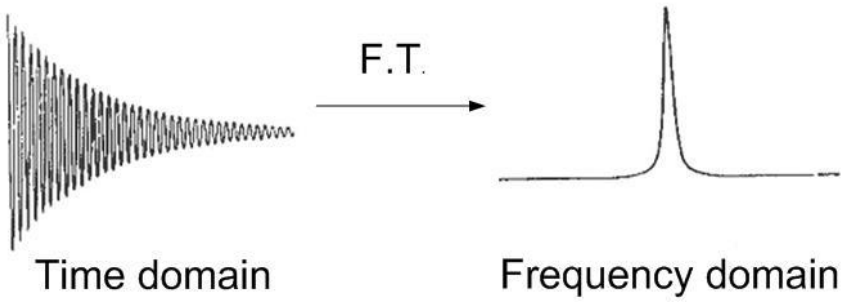

Figure 1-5. Illustration of the time domain free induction decay (FID) signal and the frequency domain NMR line after Fourier transformation (F.T.).

different effects due to differences in electron distribution, (*i.e.* magnetic fields of $(B_0 - B_e)$). As an example, signal from the ^{1}H nuclei in an H_2O molecule will appear at a slightly different frequency than that for the same nuclei in a CH_3 molecule because of chemical shift. The frequency differences are sufficiently large to detect and distinguish nuclei in different environments. Chemical shifts expressed as frequency change are dependent on the strength of the magnetic field. To provide an unambiguous comparison of chemical shift that is independent of field strength, a ratio of the measured frequency shift to the operating frequency of the magnet is taken as

$$\delta^*(ppm) = \frac{\omega - \omega_{ref}(Hz)}{\omega_{op}(MHz)}$$

(10)

where δ^* is the chemical shift in ppm, ω is the measured frequency, ω_{ref} is a reference frequency, and ω_{op} is the operating frequency of the magnet. The reference frequency is usually taken as the frequency of a compound known as TMS. Because there is a standard reference used for chemical shift as well as a lack of dependence on magnetic field strength in ppm, chemical shift can be used universally to give important information about the composition of the molecule under observation. There are countless applications of nuclear magnetic resonance which include ways to determine physical, chemical, electronic, structural, and dynamic properties of molecules. This brief overview is intended to set up basic theory behind the application of interest used to study translational dynamics of lipid molecules, pulsed-field gradient NMR.

Pulsed-Field Gradient NMR: Theory

Pulsed-field gradient NMR spectroscopy allows for direct measurements of mean square displacement (MSD) as well as of the related diffusivity and the diffusion propagator. The technique is based on the application of an external magnetic field with amplitude B_{ext} which is superimposed on the B_0 field and which is heterogeneous along the z-axis ($B_{ext} = gz$, where g is the magnetic field gradient and z is the coordinate along the z-axis). This magnetic field gradient g leads to a dependence of the Larmor frequency on the position of the nucleus. This frequency is described as

$$\omega = \gamma(B_0 + gz). \tag{11}$$

The application of magnetic field gradients allows for the detection of a change in nuclear position in the sample along the z-direction.

The PFG NMR spin echo sequence (Figure 1-6) was first used to measure self-diffusion.[92] This sequence consists of two rf pulses ($\pi/2$ and π) each followed by a gradient pulse. The first rf pulse creates transverse magnetization with phase accumulation of zero indicating complete phase coherence. The first gradient pulse

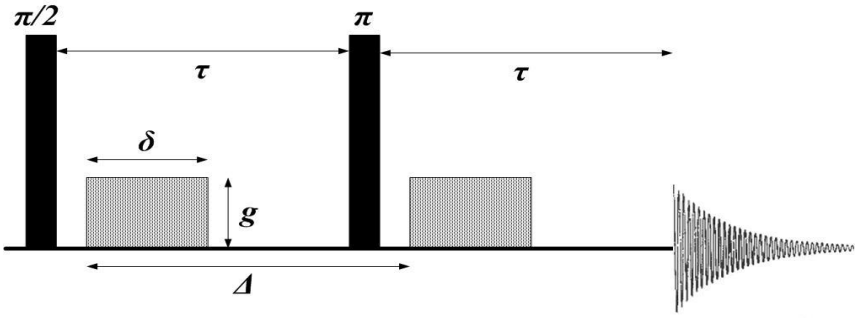

Figure 1-6. The PFG NMR spin echo sequence. Two rf pulses create transverse magnetization and then flip the direction of the spin while magnetic field

gradients of amplitude, g, and duration, δ, are applied to label and unlabel the position of the nuclei.

with amplitude *g* and duration δ is applied which labels the location of the nuclei by dephasing the magnetization which assigns a non-zero value for phase accumulation. The magnetization phase angle accumulated by each nuclear spin during the application of a gradient pulse, ***φ(t)*** is described as

$$\varphi(t) = -\gamma \int_0^t (B_0 + gz)dt \tag{12}$$

assuming that their positions, *z*, do not change during the time in which the gradients are applied. The durations of gradient pulses are relatively short so the assumption that no diffusion occurs during the time which the magnetization is dephased by the gradients is reasonable. The two gradient pulses are separated by a predetermined observation time known as the diffusion time (***Δ***) in which the nuclei are expected to change their position. Just before the second gradient pulse, a rf pulse reverses the direction of the precession. The second gradient pulse then "unlabels" the nuclei by rephasing the magnetization and reads the change of the positions along the z-direction. The change in phase accumulation is described by

$$\Delta\varphi_{z_1} = -\gamma\left\{\int_0^{\tau}(B_0 + gz_1)dt - \int_{\tau}^{2\tau}(B_0 + gz_2)dt\right\} = \gamma g\delta\Delta z \tag{13}$$

where z_1 is the position of the nucleus when the first gradient is applied, z_2 is its position when the second gradient is applied and $\Delta z = z_2 - z_1$. If the nuclei do not change their positions during the diffusion time ($\Delta z = 0$), the change in phase accumulation due to the applied gradient *g* would be zero, and the spatially dependent term of the frequency would disappear. In this case the measured NMR signal would not be reduced due to

application of the gradients.[93] For the case when Δz is not equal to zero, a non-zero value of $\Delta\varphi_{z_q}$ leads to attenuation of the measured NMR signal. The spin echo attenuation for all spins starting out at z_1 can be written as

$$\Psi = \int \cos\left(\Delta\varphi_{z_1}\right) P\left(\Delta\varphi_{z_1}\right) d\Delta\varphi_{z_1} \tag{14}$$

where $P\left(\Delta\varphi_{z_1}\right)$ the phase distribution for spins with an initial position z_1. This distribution term is determined by the distribution of Δz (Eq. 4) and is described by a Gaussian function. Equation 14 can then be written as

$$\Psi_{z_1} = \exp\left(-\left\langle \Delta\varphi_{z_1}{}^2 \right\rangle / 2\right) \tag{15}$$

where $\left\langle \Delta\varphi_{z_1}{}^2 \right\rangle$ is the average of $\Delta\varphi_{z_1}{}^2$ over the displacements Δz. This average is written in terms of mean square displacement $\left\langle z^2 \right\rangle$ as

$$\left\langle \Delta\varphi_{z_1}{}^2 \right\rangle = (\gamma\delta g)^2 \left\langle z^2 \right\rangle \tag{16}$$

Eq.15 is expected to hold for any initial position. Hence, it describes the overall attenuation in a macroscopic sample. The total spin echo attenuation for all spins Ψ due to the application of the gradient pulses is then

$$\Psi = \exp\left(-(\gamma\delta g)^2 t_{eff} D\right) \tag{17}$$

where t_{eff} is the effective diffusion time. For cases such that the duration is much smaller than the time between the application of the first gradient and that of the second (*i.e.*, $\delta << \Delta$), the effective diffusion time can be taken as Δ. In a typical PFG NMR diffusion experiment, the attenuation of signal is measured as a function of one of the experimental parameters such as *g* or τ for the purpose of finding the experimental diffusion coefficient. Details on experimental procedures will be given later in the text.

Equation 17 describes the relationship between experimental parameters such as effective diffusion time and gradient duration and amplitude with the diffusion coefficient, *D*, and attenuation in the absence of NMR relaxation. For the PFG NMR spin echo sequence, the measured signal is reduced by a factor of $\exp\left(-2\tau/T_2\right)$ due to T_2 relaxation. Under conditions where the NMR relaxation times are sufficiently long, terms that describe their effects for a given PFG NMR pulse sequence can be neglected as they have been in derivations up to this point. In some cases, these effects cannot be completely neglected. For this reason, it is more practical to measure the signal attenuation as a function of the amplitude of the gradient rather than the value of τ for diffusion experiments. In 1970, Tanner published a paper describing the stimulated echo (STE) sequence (Figure 1-7) as a useful tool for NMR diffusion studies for systems in which $T_1 > T_2$.[94] In the stimulated echo sequence, the π pulse from the spin echo sequence is split into two $\pi/2$ pulses to reduce the effects of T_2 NMR relaxation. The signal is reduced by $\exp\left(-2\tau_1/T_2\right)$ and $\exp\left(-\tau_2/T_1\right)$ due to T_2 and T_1, respectively. The measured signal is susceptible to the affects of T_2 NMR relaxation while the magnetization is in the *xy*-plane. During the time interval between the latter $\pi/2$ pulses of the stimulated echo sequence, the signal is reduced only by T_1 NMR relaxation effects. This allows for studies of systems with significantly short T_2 times to be performed over a large range of diffusion times including diffusion times >> T_2. Long diffusion times are desirable in systems with low diffusivities since for short diffusion times, even after application of the largest possible gradient, attenuation of the signal

might not be sufficiently large to properly determine diffusivity(ies). In cases of restricted or partially-restricted diffusion, there is a dependence of diffusion behavior on diffusion time and this should be studied over a range of diffusion times.[94] Under conditions of short T_2 times and/or requirements for long diffusion times, the PFG NMR stimulated echo sequence offers clear advantages over the PFG NMR spin echo sequence. Thus, the PFG NMR stimulated echo sequence is one of the most commonly used diffusion pulse sequences that determine diffusivities of lipids in membranes.

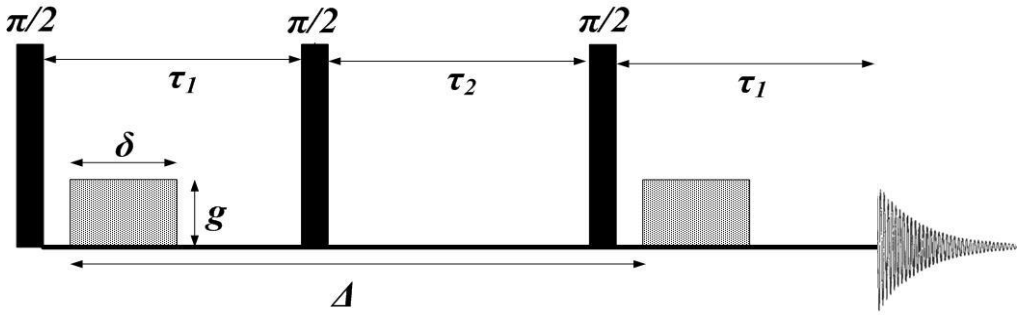

Figure 1-7. The PFG NMR stimulated echo sequence. This sequence stores the magnetization along the negative z-axis by splitting the π radiofrequency pulse in the standard spin echo sequence into two $\pi/2$ radiofrequency pulses. This sequence is very advantageous for systems in which T_2 NMR relaxation time is much shorter than T_1 NMR relaxation time.

The next PFG NMR diffusion sequence of interest to this work is the PFG NMR stimulated echo longitudinal encode-decode sequence (STE LED). A schematic of this sequence is shown in Figure 1-8. The advantage of this sequence is that it is designed to minimize effects of gradient eddy currents. Eddy currents are currents that are induced by changing magnetic fields. They can have very disturbing effects on diffusion experiments, especially when large magnetic field gradients are switched on or off. Normally, the gradient stabilization delay can be set to a value that is sufficiently long to

allow for any eddy currents produced by the gradients to dissipate after the gradient is switched off. However, this delay increases the effect of T_2 because the T_2 NMR relaxation process remains during the gradient stabilization delay. The PFG NMR STE LED sequence applies an LED delay just before acquisition to allow for eddy currents to die out. Only T_1 NMR relaxation occurs during this delay. With this LED delay, the gradient stabilization time can be set to a value much smaller than that required for the standard STE sequence. This sequence is most beneficial for use with samples that are limited by extremely short T_2 relaxation times.

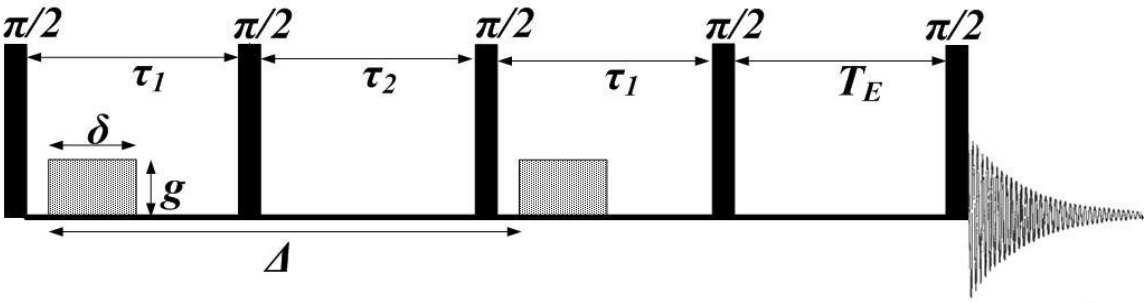

Figure 1-8. The PFG NMR stimulated echo longitudinal encode-decode sequence. The sequence adds an additional delay at the end of the standard PFG NMR stimulated echo sequence. During this delay, the magnetization is stored along the z-axis and, a spoiler gradient can be applied to reduce any effects from eddy currents.

The last PFG NMR diffusion sequence that is of interest to this work is known as the 13-interval sequence. This sequence incorporates alternating (bipolar) gradients in contrast to the previous sequence, where the gradients were strictly unipolar. This sequence is shown in Figure 1-9. Alternating pulsed-field gradients are used to suppress susceptibility-induced artifacts in diffusion experiments. Magnetic susceptibility is related to the manner in which an object causes distortions in the applied magnetic field due to the inherent and/or geometric properties of that object.[95] Samples that are heterogeneous in nature present a specific problem due to the

existence of inhomogeneous internal magnetic fields even before the application of an external magnetic field.[96] Susceptibility-induced inhomogeneities in the local field manifest themselves in various manners including phase shifts in the frequency domain and shifts in the spin echo position in the time domain.[97] These manifestations are dependent on the strength of the applied magnetic field. For this reason, the presence of susceptibility artifacts in NMR results can be tested by directly comparing data from

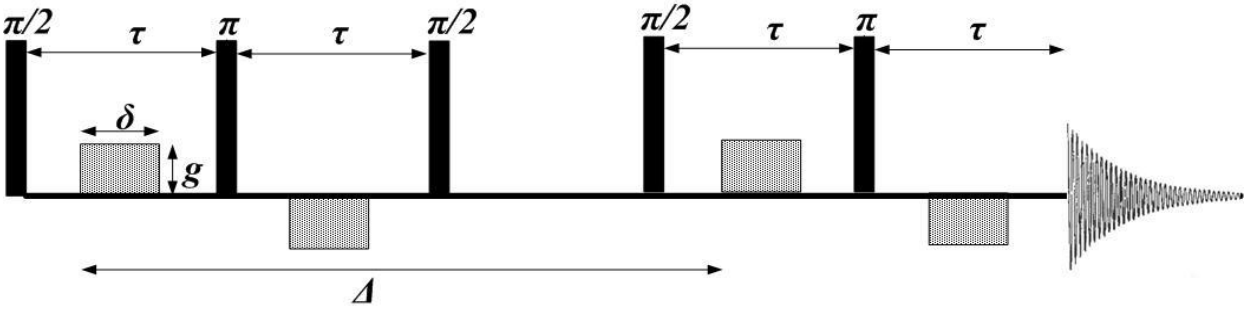

Figure 1-9. The PFG NMR thirteen-interval pulse sequence. This pulse sequence uses alternating gradients to suppress artifacts induced by magnetic susceptibility.

different B_0 field strengths. The coincidence of such data verifies the absence of susceptibility artifacts, however it is not always convenient or possible to do diffusion experiments at multiple field strengths. The 13-interval sequence is intended to minimize susceptibility distortions of the PFG NMR data. Comparison of diffusion results obtained from a 13-interval sequence with those from more standard sequences, such as the stimulated echo sequence, can be used to verify that magnetic susceptibility effects are not distorting diffusion results.

Pulsed-Field Gradient NMR: Application for Studies of Lipid Bilayers

To measure diffusivity, PFG NMR signal, *A(g)*, obtained using one of the PFG NMR sequences above is measured as a function of the magnitude of applied field gradient (*g*) under conditions where all other sequence parameters are kept constant.

For most cases, the amplitudes of the NMR lines in frequency-domain spectra of lipids as well the area under these lines were used to measure signal to obtain the PFG NMR attenuation curves. It is also possible to use the attenuation of the amplitude of the signal in the time-domain spectra to obtain PFG NMR curves. Both approaches can be used successfully for diffusion measurements. The advantage of the former approach is related to the possibility of measuring separately diffusivities associated with different NMR lines, which can originate from different types of molecules in the studied samples. This is especially relevant for the case of lipid bilayers in which there are molecules such as water with a unique chemical shift and diffusivity contributing to the measured NMR signal alongside lipid molecules with different chemical shift and diffusivity. The diffusivities *D* are obtained from either a one-exponential or two-exponential fit of the PFG NMR attenuation curves using

$$\Psi(g,\delta,t_{eff}) \equiv \frac{A(g)}{A(g=0)} = \sum_{i=1}^{n=1 or 2} p_i \exp\left(-q^2 t_{eff} D_i^m\right), \quad (18)$$

where *A(g)* is the measured signal for a given gradient strength, *A(g=0)* is the maximum gradient strength (signal for applied gradient amplitude of zero), $q = \gamma g \delta$ and p_i is the fraction of molecules diffusing with a diffusivity D_i^m. The effective diffusion time (t_{eff}) is equal to $\left(\Delta - \delta/3\right)$ for the spin echo, stimulated echo sequence, and stimulated echo LED sequences and $\left(\Delta + \frac{\tau}{4} - \frac{\delta}{3}\right)$ for the 13-interval sequence.[98,99] Eq. 18 is completely analogous to Eq. 17, however the sum of terms indicates the presence of more than one ensemble of molecules with distinct dynamics. A one-exponential (monoexponential) fit would indicate that there is one ensemble of molecules

contributing to the overall signal yielding one single value of diffusivity. A two-exponential (biexponential) fit indicates that two ensembles, with unique values for the diffusion coefficient as well as p_i fractions, contribute to the measured signal.

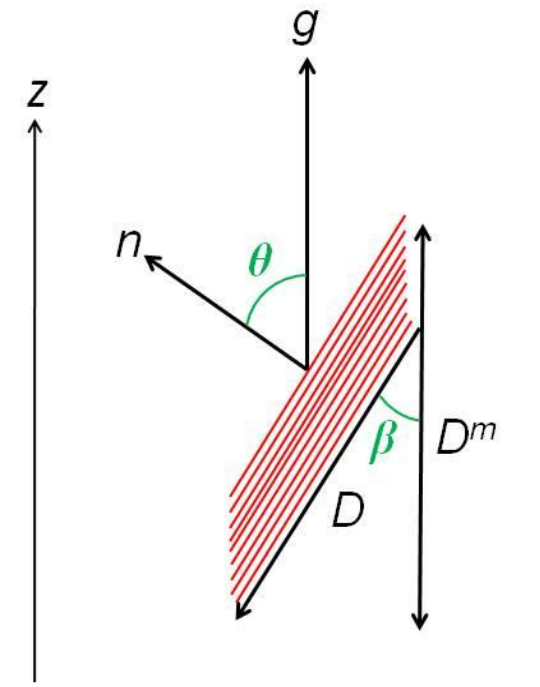

$$D = \left(\frac{1}{\cos \beta} \right)^2 D^m = 1.5 \times D^m$$

Figure 1-10. Comparison between the directions of measured and lateral diffusion. The gradients (*g*) are oriented along the *z*-axis hence any observation of the diffusion of lipids is actual diffusion along the direction in which the gradients are applied. The normal to the surface of the bilayers *n* is oriented at the angle θ. Multiplying the measured diffusion coefficient (D^m) by a factor of 1.5 yields the desired lateral diffusion coefficient (D).

The diffusivities determined by fitting the attenuation curves using equation 18 correspond to the diffusion along the direction, which coincides with the direction of the gradients and that of the B_0 field (Figure 1-10). This direction was different from that of

diffusivities ($D^m \alpha \left\langle \left(r^m\right)^2 \right\rangle$) in the plane of the lipid bilayers for reasons associated with minimizing T_2 relaxation affects. This orientation of the bilayer normal *n* and the theory behind it will be discussed in detail in Chapter 2. Ultimately, the measured diffusivities were multiplied by a factor $(1/\cos \beta)^2 = 1.5$ to determine the true lateral diffusion of lipids along the bilayer.[90] In this calculation we have assumed that the displacements of lipids in the direction perpendicular to the bilayer surface are negligibly small in comparison to the corresponding displacements along the bilayer surface. Detailed analysis of diffusion coefficients obtained from PFG NMR measurements will be discussed in more detail in the presentation of results in Chapter 3.

CHAPTER 2
DEVELOPMENT OF DIFFUSION MEASUREMENTS IN LIPID BILAYERS USING HIGH-FIELD, HIGH-GRADIENT PFG NMR

Development Associated with Planar-Supported Lipid Bilayer Samples

A wide variety of model membranes differing in composition and structure have been utilized extensively for studies of membrane dynamic and structural properties. The primary lipid components of biological and model membranes include phospholipids, sphingolipids, and sterols. While membranes composed of a single lipid or binary mixtures of lipids have been well characterized, ternary mixtures of the three main membrane components represent a better model of the eukaryotic membrane. Common eukaryotic membranes are composed of about 50 mol% phospholipids and sphingolipids and up to 40 mol% of cholesterol.[22] Formation of domains have been found to be strongly promoted by the presence of two types of lipids with phase transition temperatures which are very different from each other.[22] Lipids that contain charged headgroups have also been incorporated into model membranes to mimic the charged nature of certain cell membranes. While lipid charge has been shown to have an effect on domain formation, this effect is not significant.[22] Lipids bilayers can be readily constructed in the form of vesicles and planar structures. The use of lipid bilayers reconstituted on planar substrates is common practice for many of these studies of membranes. Planar-supported bilayer samples are well-defined and the absence of the orientational distribution of the membrane planes in such samples offers many advantages for research. Membranes reconstituted on solid supports such as silica have been observed to retain the lateral fluidity associated with lipid membranes in vesicles and cell membranes.[100] These types of membrane samples are especially attractive to those interested in investigations of reconstituted functional membrane

molecules such as proteins and receptors.[100-102] The potential for planar-supported lipid bilayers to be used as biosensors gives a practical applicability to the membrane. For those interested in studies of translational dynamics of membrane constituents, planar-supported membranes are advantageous because of the well-defined orientation of the bilayer plane.[101] In this work multibilayer stacks of lipid bilayers are reconstituted on solid support as shown in See Figure 2-1. Each support holds on the order of 1000 bilayers each separated by a thin layer of water about 2 nm thick.[103,104] For studies of lateral diffusion, these samples offer an advantage over bilayers of vesicles, either unilamellar or multilamellar, related to the absence of curvature of the bilayer. Curvature in the bilayer can complicate the interpretation of diffusion results which are obtained along a fixed microscopic direction coinciding with the direction of the applied gradients (*i.e.*, the measured diffusion coefficient for a lipid diffusing in a curved membrane could be smaller than the true diffusion coefficient due to misinterpretation of the measured mean square displacement). Also, planar membranes reconstituted on glass plates allows for the microscopic orientation of lipids in the bilayer to address problems associated with T_2. In contrast to samples where a single bilayer (or monolayer) is reconstituted on a solid support, the use of multibilayer stacks addresses any concerns associated with the influences of lipid-support interactions. These effects can be neglected because the number of bilayers that are in contact with the solid supports are very small in comparison to the many thousands of bilayers between each support. Also, in comparison to these planar-supported bilayers, the use of multibilayer stacks on solid support provides sufficiently large NMR signal for PFG NMR measurements.

Preparation of Planar-Supported Multibilayer Stacks

PFG NMR studies were performed with multibilayer stacks supported on thin glass plates. The bilayer stacks were prepared from ternary lipid mixtures of either 1,2-dioleoyl-*sn*-glycero-3-phosphocholine, (DOPC, >99%), Chicken egg yolk sphingomyelin, (SM, >95%), and cholesterol, (CHOL, >99%) in equimolar proportions or DOPC, 1,2-dipalmitoyl-*sn*-glycero-3-phosphocholine (DPPC, >99%), and CHOL with the composition of 30% sterol and equimolar amounts of DOPC and DPPC. DOPC and DPPC were purchased from Avanti Polar Lipid, Inc. (Alabaster, AL, USA), while SM and cholesterol were supplied by Sigma-Aldrich (St. Louis, MO, USA). Two protocols, which are adapted from the current literature,[91,105] are used for the preparation of model lipid membranes in this work. In both techniques a lipid film is deposited on thin glass plates, which is followed by hydration causing self-orientation of the lipids into multibilayer stacks. The lipids are individually dissolved in solvents and combined using the appropriate volume ratios to create a final ternary lipid solution. This solution is deposited onto clean glass plates (5×5mm^2 or 6×7 mm^2 with a plate thickness of ~0.1 mm) obtained from Marienfeldt/Menzel (Lauda-Königshofen/Braunschweig, Germany) and the solvent is evaporated off overnight under high vacuum at ~313 K. Of the two methods employed here, the differences lie mainly in the solvents used to dissolve the lipids and in the way of introducing water into the system, *i.e.* either directly as liquid water or from the gas phase. The two techniques will be discussed separately from this point on. It was observed in this work that the PFG NMR data obtained with samples prepared using these two techniques were not influenced by the preparation method within the experimental uncertainty. Verification of the orientation of lipids in bilayers as well as reproducibility issues will be discussed in future text. In the first method, a

solution of methanol:1-propanol (1:4 vol:vol) is used as the solvent. The ternary lipid solution was deposited on the glass plates to a sample mass of 8-9 μg/mm^2. After

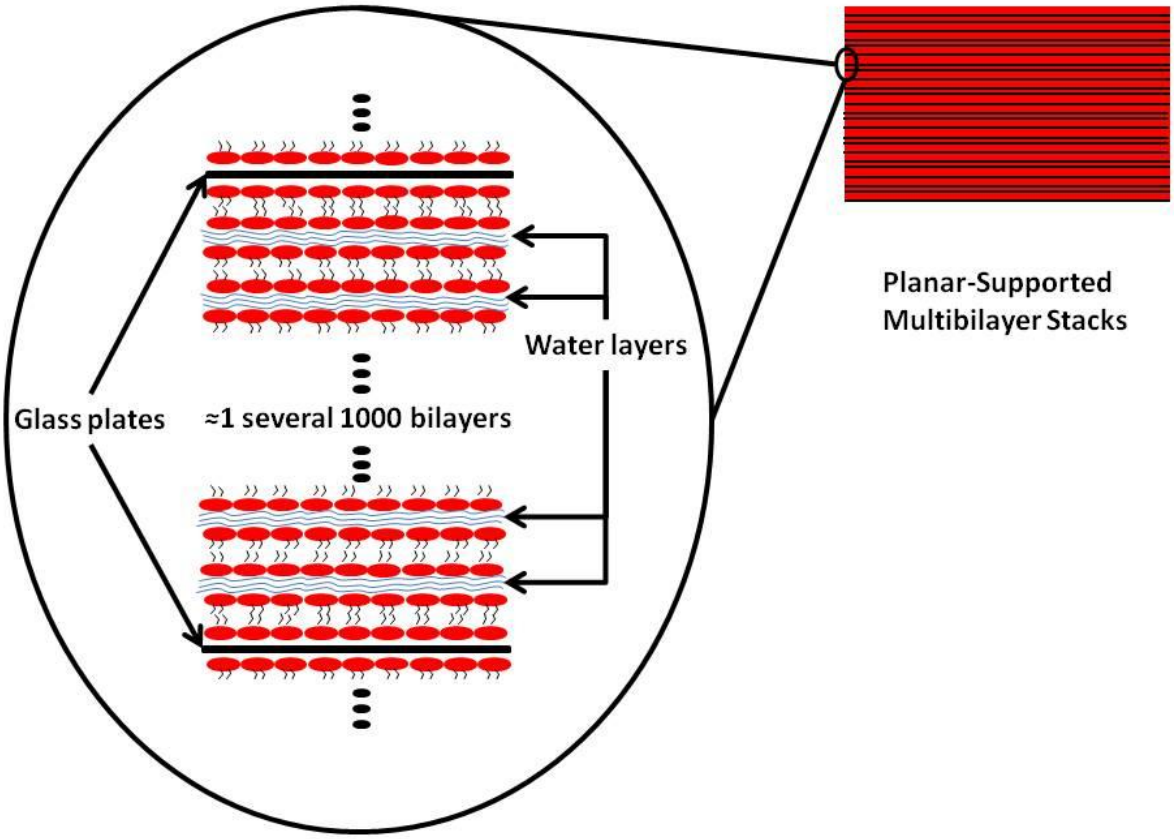

Figure 2-1. Illustration of a PFG NMR sample consisting of many planar-supported multibilayer stacks. The figure zooms in on the stack to show that many bilayers (*i.e.*, on the order of 1,000) are reconstituted on each glass plate. Each bilayer is separated by a thin layer of free water about 2 nm thick.

solvent evaporation, from 30 to 40 plates were stacked on top of each other and transferred to a hydration chamber filled with ^2H_2O saturated with K_2SO_4. The salt and ^2H_2O were obtained from Sigma-Aldrich (St. Louis, MO, USA) and Spectra Stable Isotopes (Columbia, MD, USA), respectively. In this method, the hydration takes place only from the gas phase (*i.e.* indirectly) under the condition of a relative humidity of around 97%. The salt solution is used to keep the humidity slightly below 100% to

ensure that condensation of liquid water domains on the glass plates with lipids does not occur. This prevents direct contact between the lipid films on glass plates and liquid ^2H_2O. The stack was left in this environment for seven days at 313 K for equilibration. Once the stack is set up inside the NMR tube (see next section for details), pure ^2H_2O is added to bring the sample to maximum (i.e. 100%) hydration and to keep it at this hydration.

The second method uses a solution of chloroform:methanol (2:1 vol:vol) as the solvent. The ternary lipid solution was prepared as discussed above using three individual lipid stock solutions. A sublimable solid, i.e. naphthalene obtained from Cambridge Isotope Laboratories (Andover, MA, USA), was then introduced into the lipid mixture in a naphthalene:lipid molar ratio of 1:1. The resulting solution was deposited onto the glass plates to a sample mass of 8.3 $\mu g/mm^2$. After solvent evaporation, the plates were left unstacked. They were hydrated from the gas phase in the presence of liquid ^2H_2O saturated with K_2SO_4 for 1-2 days inside of the hydration chamber. After the initial hydration step, pure liquid ^2H_2O was directly added to the lipid bilayers using a syringe to achieve a final molar ratio of ~28 moles of water per mole of lipid. The direct hydration by pure ^2H_2O is expected to bring the sample to maximum hydration of 100%. 35-40 plates were stacked and wrapped in parafilm. The stack was then held at 277 K for additional 1-2 days. Once the stacks were fully prepared and hydrated, they were transferred to an NMR tube with an external diameter of 10 mm (for studies using 750 MHz (17.6 T) PFG NMR spectrometer) or 7.5 mm (for studies using 400 MHz (9.4 T) and 125 MHz (2.9 T) PFG NMR spectrometers.

Here, two protocols are presented for preparation of multibilayer stacks. Orientation of lipids in multibilayer stacks was verified using the first protocol described in this section. The second protocol gave sufficiently similar proton NMR spectra in terms of shape, linewidth, and chemical shift. This observation shows that also the second protocol results in preparation of samples of oriented multibilayer stacks because ^{1}H NMR spectra are sensitive to the extent of the lipid self-organization into oriented bilayers as will be discussed later. Most multibilayer stacks were prepared using the second protocol which uses the sublimable solid, naphthalene in order to promote better orientation. Naphtalene is believed to randomly distribute among lipids when the solvent solution is dried on the glass.[105] After overnight vacuum-drying, the solid is gone leaving the samples more amenable to hydration[105] providing a better extent of orientation and a more effective sample preparation protocol. It was observed that this method gave a better sample preparation reproducibility yielding a lower probability of unusable samples where a significant fraction of lipids did not form the bilayers or were not ideally oriented in the bilayer.

Sample preparation methods for bilayers reconstituted on glass planar supports have been considered tedious[106] and very sensitive to solvent choice and hydration techniques[107]. Evaluation and adaptation of protocols were based off of issues with lipid mixture spreadability and hydration issues. Great care was taken when using these protocols to prevent untimely solvent evaporation and contamination. Exposure to air was kept to a minimum to prevent lipid oxidation. Lipid oxidation is more likely to occur when lipids are directly exposed to air, *i.e.*, when there is no or vary little water or solvent. The lipids were stored in a way allowing minimizing the exposure to air and dry

lipid mixtures (*i.e.*, after solvent evaporation and before hydration) were kept under vacuum whenever possible. Mass spectroscopy measurements revealed no changes in the lipid composition of the lipid mixtures obtained from the bilayer samples used for diffusion measurements in comparison to the original lipid mixtures that were used to prepare the samples. These measurements were performed by Konstantin Ulrich. Oxidation was seen to have an insignificant affect on the samples if proper measures were taken.

Orientation of Planar-Supported Multibilayer Stacks at the Magic Angle

^{1}H PFG NMR measurements of lipids in lipid membranes are complicated by rather short transversal (T_2) NMR relaxation times and the related large line width in a frequency-domain. Short T_2 times and the related line broadening are mainly caused by strong proton dipole-dipole interactions in lipids that are not completely averaged by molecular motion. In order to minimize the effects of dipole-dipole interactions on T_2 times and the line width, the following main three options have been used or at least discussed in the literature: (*i*) PFG NMR studies can be carried out using oriented samples, *i.e.*, multibilayer stacks oriented along the so-called “magic” angle (54.7º) with respect to the direction of the applied magnetic field[88,90,91] (*ii*) PFG NMR can be combined with a magic angle spinning (MAS) technique,[46,87,108,109] *viz*. fast sample rotation along the direction given by the magic angle and (*iii*) PFG can be combined with multiple-pulse homonuclear decoupling.[110] The MAS approach has proven to be an especially powerful method allowing for the discrimination between different membrane components. Unfortunately, it is not technically compatible with an application of commercially-available high gradient systems. As it is not a trivial task to create reliable and reproducible magnetic field gradients of such high amplitudes, it is imperative to

utilize what is available commercially. Similarly, approach (*iii*) is not compatible with the application of high gradients because measurement artifacts are likely to occur if high gradient amplitudes necessary for submicron diffusion measurements are superimposed on the decoupling radiofrequency pulse sequence.[110] Approach (*i*) gives the possibility of adapting PFG NMR diffusion studies using high magnetic field gradient amplitudes for investigations of lipid transport in bilayers which are severely limited by short T_2 relaxation times.

In order to minimize dipole-dipole effects on transverse relaxation, a sample insert had to be created to macroscopically orient the bilayers in NMR spectrometers. The stack of glass plates with bilayers should be oriented in such a way that the angle (θ) between the dipole moment of lipids and the direction of the applied magnetic field B_0 is very close to the so-called "magic" angle (54.7°). In this case, the scaling factor ($3\cos^2\theta$-1) in the Hamiltonian term describing the dipole-dipole interaction approaches a zero value. To orient the bilayer stacks at the magic angle a special insert was originally developed by Konstantin Ulrich, a previous graduate student working for Dr. S. Vasenkov at the Universität Leipzig in Leipzig, Germany. It was designed for use with 125 and 400 MHz spectrometers. The same approach was used to make inserts suitable for the current work using 750 MHz spectrometer. Figure 2-2 shows schematic presentation of the insert. The insert is made of plexiglass and fits into 10 mm NMR tubes used in this study. The stacks were placed in the insert and inside the tube. Before sealing the NMR tube with a lipid sample, a few drops of excess ^2H_2O are added on the tube walls above or below the sample to ensure that the relative humidity in the

gas phase surrounding the bilayers is 100%. Verification of macroscopic orientation of multibilayer stacks will be discussed in detail later in Chapter 2.

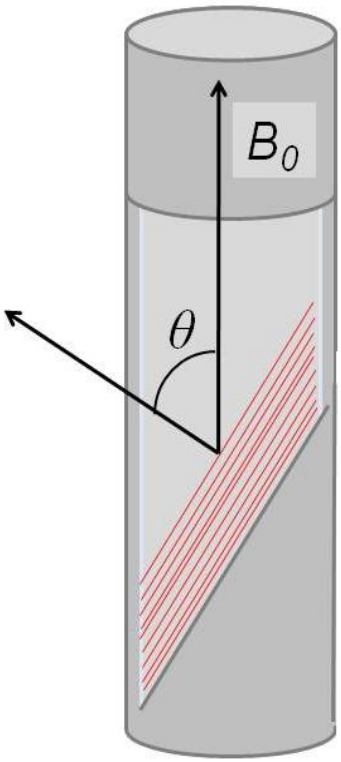

Figure 2-2. Schematic of the magic angle insert. The insert orients the multibilayer stacks such that angle (θ) between the dipole moment of the lipids and the direction of the external magnetic field (B_0) is equal to the magic angle. Orientation at the magic angle leads to a minimization of dipole-dipole interaction effects on T_2 NMR relaxation.

Development Associated with PFG NMR Diffusion Experiments

The majority of measurements of self-diffusion in model lipid bilayers were carried out on a wide-bore Bruker PFG NMR spectrometer operating at a ^{1}H resonance frequency of 750 MHz (17.6 T). This spectrometer is located at the Advanced Magnetic

Resonance Imaging and Spectroscopy (AMRIS) facility of University of Florida in Gainesville, Florida. A Diff60 probe with GREAT60 amplifier was used to generate high gradients for diffusion measurements using the 750 MHz spectrometer. Initial experiments were conducted at a lower frequency by and in collaboration with Konstantin Ulrich. These measurements were carried out using two different home-made spectrometers: PFG NMR spectrometers FEGRIS NT and FEGRIS FT operating at a ^{1}H resonance frequency of 400 MHz and 125 MHz, respectively. Discussion of measurements conducted at 400 MHz and 125 MHz is limited to this section for early development and verification purposes. Acquisition of each proton spectrum using the PFG NMR sequences required up to 240 scans. The resulting ratios of signal to noise or to the background signal at small gradient strengths were around 300 for the measurements at 750 MHz and in the range of 50 for the measurements at 400 MHz and 125 MHz. Temperatures were varied in the range of 291 K to 310 K. The diffusion probes used at 750 MHz are suitable for PFG NMR measurements with gradient amplitudes up to 35 T/m, but a maximum of only 28 T/m was needed for most experiments.

Calibration Experiments

Before carrying out diffusion measurements it is necessary to ensure that the amplitudes of the gradients generated by the gradient coils are known with a very high precision. The most common approach is to conduct PFG NMR experiments determining the diffusion coefficient for a species with a well-known diffusivity.[111] ^{1}H PFG NMR calibrations measurements were carried out with two liquids, water and glycerol. Figure 2-3A gives an example of an attenuation plot for diffusion experiments conducted in order to calculate the diffusion coefficient of a small amount of H_2O in

liquid D_2O. Protonated water (H_2O) is diluted in deuterated water (D_2O) in order to decrease the number of NMR-active nuclei under study and thus make the signal amplitude closer to that in lipid samples. The standard PFG NMR stimulated echo sequence was used with δ = 1.1 ms for two different diffusion times, t_{eff} = 14.63 and 39.63 ms. The gradients were varied between 0.396 and 2.00 T/m. In similar experiments, the diffusion coefficient was measured for t_{eff} as large as 240 ms (not shown). The diffusivity of deuterated water at a given temperature is well known and can be used for the calibration of the applied gradient amplitudes. The relationship between gradient amplitude and diffusivity can be found to be proportional according to the attenuation equation (Eq. 18) such that

$$D_{H_2O} g_{H_2O}^{\ 2} = D_{lit} g_{act}^{\ 2} \tag{18}$$

where D_{H2O} and D_{lit} is the measured and literature values for the diffusion coefficient of the water sample, respectively, g_{H2O} is the gradient amplitudes given by the software of the spectrometer (i.e. the gradient amplitude that was used to determine D_{H2O}) , and g_{act} is the actual gradient amplitudes. At room temperature (298.2 K), diffusivity is expected to be 1.9×10^{-9} m^2/s for pure D_2O and 2.3×10^{-9} m^2/s for pure H_2O. Since the concentration for protonated water was sufficiently small, the value for pure deuterated water was used for calibration. The gradient calibration constant (GCC) must be adjusted such that results from diffusion experiments on water (H_2O diluted in D_2O) yield that value. This ensures that actual gradient amplitudes that are applied in diffusion experiments correspond to those used for the calculation of diffusion coefficients.

The PFG NMR measurement of glycerin serves to verify the linearity of the gradients (*viz.* proportionality between the actual gradient applied and the input value of the gradient as shown by the software of the spectrometer) at large gradient amplitudes and durations. Figure 2-3B show examples of attenuation plots for diffusion experiments conducted for glycerin. The figure also shows the agreement of results obtained from the most standard PFG NMR diffusion sequence, the stimulated echo, with results obtained using the PFG NMR spin echo, stimulated echo LED, and the 13-interval sequences. These comparisons were performed to ensure that each sequence gave reliable results for a standard homogeneous sample with a diffusivity similar to that in lipid samples. Verification of each sequence was conducted separately (*i.e.*, on different days), often using slightly different experimental parameters and sometimes different samples. Most of the results were obtained for each sequence with $\delta \cong 3.0$ ms, gradients ranging from 0.33 – 24.1 T/m, and t_{eff} as small as 5 ms and as large as 240 ms. Each sequence produced results that were in agreement with the results obtained with the stimulated echo sequence within the experimental uncertainty. The data then indicates that the sequences operate properly and do not produce disturbing artifacts, even at very large gradient strengths. The diffusivity of glycerol at room temperature is expected to be around 2×10^{-12} m^2/s (similar to lipid samples). The experimental diffusion coefficients agreed with this value within experimental uncertainty. In the case of glycerin measurements the actual value of diffusivity is not of primary interest. Instead, the focus was on the shape of the attenuation curve. Measured attenuation curves should remain monoexponential (as is expected of homogeneous liquids) even with the use of large duration and amplitudes of the

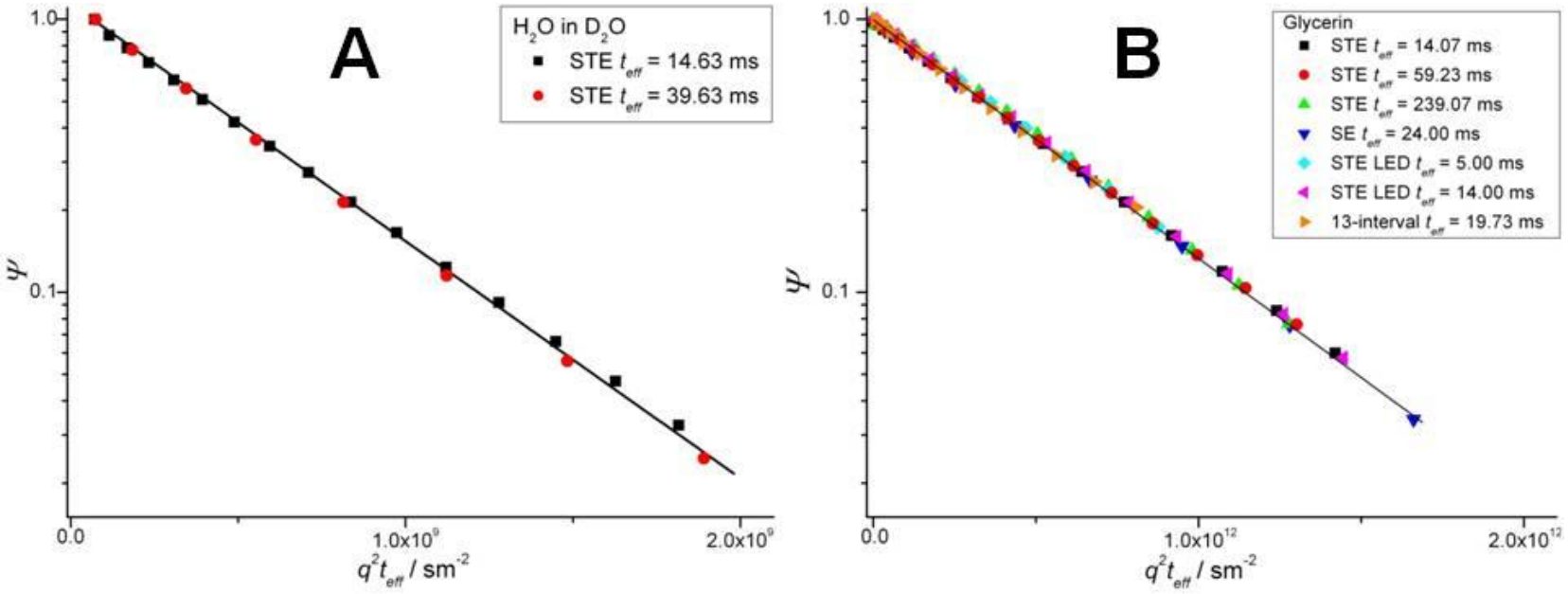

Figure 2-3. Examples of PFG NMR attenuation plots for water (A) and glycerin (B). The measured diffusion coefficient of water is compared to known values and used to calibrate gradient amplitudes. Experiments conducted on glycerin served to test the linearity of the gradients at high magnetic field gradient amplitudes as well as to confirm the agreement of results obtained from different PFG NMR diffusion sequences.

gradients used. In Figure 2-3B, it is seen that the attenuation of signal remain monoexponential throughout the range of gradients which are applied. Diffusion studies of glycerin at room temperature confirm that the gradients behave linearly even at high magnetic field gradient amplitudes and that there should be no artifacts in experiments associated with the choice of diffusion sequence.

Addressing Limitations Concerning Gradient Pulses

Studies of lipid self-diffusion in heterogeneous lipid bilayers, especially those which form small liquid-ordered domains as discussed in Chapter 1, involves the measurement of short displacements as well as small diffusivities. In order to measure lipid diffusivities which are as low as 10^{-13} m^2/s, it is necessary to apply gradients with sufficient amplitudes and/or pulse durations to measure an acceptable level of signal attenuation. The short T_2 NMR relaxation times of lipid molecules in bilayers limit the duration of the gradient pulse. Also, for studies observing anomalous or restricted diffusion, PFG NMR measurements fail to give correct information about dynamics if the conditions of the narrow-pulse approximation[112,113] are not fulfilled. These conditions are: (*i*) the trajectory length over the duration of the gradient (*i.e.*, MSD as defined by Eq. 5) has to be small in comparison with the size of restriction (*i.e.*, domain), and (*ii*) the effective diffusion time has to be sufficiently larger than the gradient pulse duration ($t_{eff} >> \delta$). Large gradient amplitudes are applied to compensate for limitations on gradient pulse durations. The use of high gradients and relatively short gradient durations imposes complications when considering the relationship between the input gradient pulse and the actual pulse that is applied in an experiment. These complications were addressed by adjusting the gradient shape, the delay for gradient recovery, and parameters used to account for eddy currents known as preemphasis

adjustment. The development discussed in this section is novel for high field, high-gradient PFG NMR studies used to measure lateral dynamics of lipids in model membranes.

Gradient pulse shape and delay for gradient recovery

Until now in this text, the gradient pulse has been depicted as a perfect square-shaped pulse. In reality, it is virtually impossible to apply a gradient such that the amplitude of the value rises instantaneously from zero to some arbitrary value. Pulsed-field gradients are generated by pulses of electric current flowing through a gradient coil. Sharp rise and fall times (*i.e.*, rapid increase and decrease of current form the current source)[93] of a square pulse can create disturbing responses such as overshoot which are very erratic and cannot always be controlled and reproduced. These responses promote induction of eddy currents which cause measurement artifacts that are not always negligible in comparison to the actual data. It is important to have very consistent and reproducible gradient pulses in order to minimize artifacts and measure true diffusion behavior. Shaped pulses are common alternatives to the generic square gradient pulse. Often, sine- and trapezoidal-shaped pulses allow for a more gradual climb towards the maximum gradient amplitude.[79] Eddy currents induced by the application of magnetic field gradients can be reduced by shaped gradient pulses but it is still important that the shape itself is free of distortion.

In order to produce the optimal gradient pulse which is free from shape distortion and eddy current effects, it was necessary to explore various types of shapes that would simultaneously (*i*) provide the quickest path to the full amplitude of the gradient, (*ii*) provide the largest area under the gradient pulse, and (*iii*) be sufficiently reproducible and free from distortions. In order to explore the suitability of different shapes, a digital

oscilloscope was used to directly observe the shapes of the gradient pulses. The oscilloscope gave information about the gradient pulse shape, which allowed for the observation of a difference (if any) between the shape prescribed by the software and the real shape of the gradient pulses. A pulse with a shape of a sine wave from 0 to π was observed to be easily and accurately reproducible. It is most advantageous, however, for very short gradient durations. For short durations, a sine wave will reach the full amplitude in a short amount of time and provides an efficient pulse area close to that for a square pulse. Longer pulses require shapes that have a sufficient plateau at full amplitude much like the square pulse. Trapezoidal-shaped pulses provide the opportunity to designate ramp up, ramp down, and plateau durations. With this shape, it is possible to control and optimize each part of the shape. The linear ramps leading to and from the plateau create a more gradual path in contrast to the instantaneous switching on and off of the square pulse. It was necessary to determine the minimum durations for the ramp up and ramp down portions of the shape that can be followed by the hardware and do not lead to disturbing eddy currents. These values were found to be around 500 μs for gradient amplitudes as large as 25 T/m, which was considered to be reasonable for experimental parameters. Next, the ramp curves were replaced individually by $\pi/2$ sine curves in an attempt to increase area under the gradient curve. The $\pi/2$ sine was preferred over the linear ramp up curve however the difference was not significant. Replacing the ramp down curve with a $\pi/2$ sine induced distortions to the gradient shape. From these results, it was determined that the ideal gradient pulse shape was a trapezoid-like shape with a $\pi/2$ sine ramp up and a linear ramp down. For

many cases such as in the 13-interval sequence as well as other diffusion measurements, a standard trapezoid (linear ramp up and down) was sufficient.

In order to ensure that effects either from gradient shape distortion or induced eddy currents associated with the magnetic field gradients do not disturb diffusion measurement, it is necessary to let sufficient time pass after the last gradient pulse in the sequence is turned off and before data acquisition is started. According to observations from the oscilloscope, the delay for gradient recovery, which is that very time period between the end of the gradient pulse and the beginning of the rf pulse and/or data acquisition, must be larger than 500 μs for experimental parameters used on lipid samples. To verify that the value of delay was sufficient, a series of simple PFG NMR stimulated echo experiments with the gradient amplitudes as large as 25 T/m were carried out. The value of delay for gradient recovery was varied throughout this series of experiments. Using time intervals for delays for gradient recovery which are not sufficiently long can produce distortions in the shape in spectra as well as a reduction in amplitude. The minimum value for delay for gradient recovery is considered to be the value at which the shape and/or amplitude of the spectra stops changing. This value was determined to be at least 1 ms, which is much longer than observed with the oscilloscope.

Preemphasis adjustment and B_0 compensation

As mentioned previously, gradient pulse durations are often limited by short T_2 NMR relaxation times. In the previous section, it was discussed how the gradient shape was optimized. The minimum delay for gradient recovery was found to be a rather long value of 1 ms. Preemphasis adjustment can be used to further improve gradient pulse

shape and reduce the influence of eddy currents allowing for shorter gradient stabilization delays. Preemphasis adjustment applies corrections to the current at leading and tail edges of the gradient pulse.[79] These corrections exist in the form of three exponential functions, with different amplitude and time constants and when optimized, can further reduce the effect of eddy currents. Optimization of preemphasis parameters for diffusion studies on lipid membranes was done in collaboration with a Bruker engineer. PFG NMR stimulated echo experiments similar to those described in the previous paragraph were conducted and showed that the new parameter optimization allowed for the use of delays for gradient recovery as small as 500 μs. B_0 compensation was attempted but did not provide appreciable benefits to diffusion experiments and was ultimately not implemented.

Verification of Macroscopic and Microscopic Orientation of Multibilayer Stacks

The orientation of the lipids in multibilayer stacks of an equimolar mixture DOPC/SM/CHOL prepared for diffusion measurements was characterized using ^{31}P NMR by Konstantin Ulrich. Figure 2-4 shows examples of proton-decouple ^{31}P NMR frequency-domain spectra, which were recorded for different values of θ, the angle of orientation of a multibilayer stack with respect to the direction of the constant magnetic field B_0 (Figure 2-2). The angle was changed using the goniometer probe that allows performing measurements at different, well-defined values of θ. Each of the measured spectra consists of a single line with a half-width around 6 ppm. The spectra in this figure collectively demonstrate that the majority of lipids in the sample are arrange in well-oriented bilayers due to the following considerations: (i) the chemical shift of the lines depends on the values of θ, as expected for macroscopically oriented lipid

bilayers, and (ii) the line half-widths, which are mostly determined by the chemical shift anisotropy, are sufficiently small, leading to the conclusion that there is insignificant distribution of orientations of individual lipid with respect to the bilayers normal. The signal from randomly oriented lipids in the sample is expected to be independent of θ

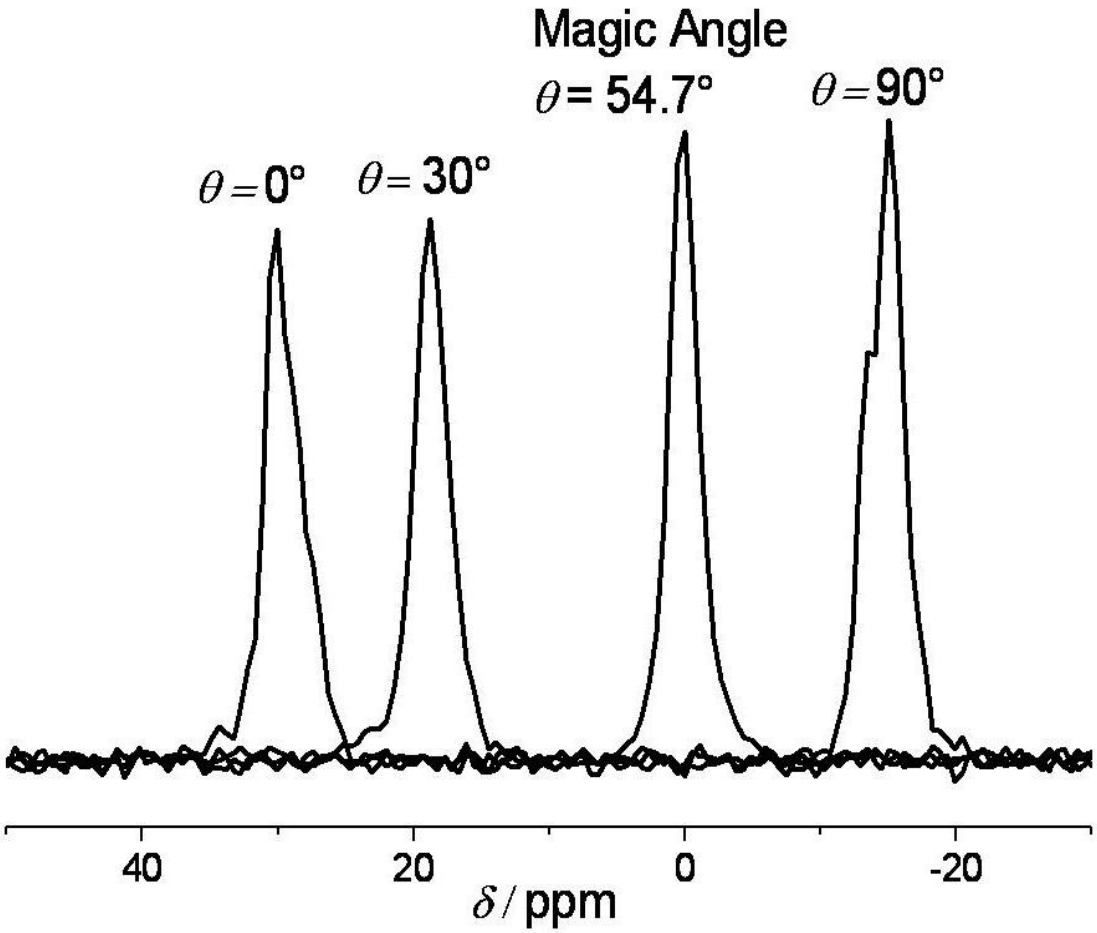

Figure 2-4. Proton-decoupled ^{31}P NMR spectra of DOPC/SM/CHOL multibilayer stacks to study the orientation of lipids in the bilayers. Each NMR line which was obtained by a Hahn echo sequence represents spectra for a different angle θ between the normal to the surface of the glass (which coincides with the direction of the dipole moment of the lipids forming bilayers) and the direction of B_0 field. The comparison shows that the signal of the lipids is dependent on θ which is not expected for randomly oriented lipids. This data was obtained by Konstantin Ulrich.

and have a half-width that is several times larger than that of the lines in Figure 2-4. Within experimental uncertainty, no such signal was observed. On the basis of the data

in Figure 2-4, it was estimated that more than 97% of lipids in the multibilayer stack samples are located in well-oriented bilayers. The extent of orientation is expected to be the same or similar within experimental uncertainty for samples prepared from different mixtures and/or by different protocols.

Macroscopic orientation of the multibilayer stacks of an equimolar mixture of DOPC/SM/CHOL in the insert with respect to the direction of the B_0 field was verified using ^{1}H NMR. This characterization was also performed by Konstantin Ulrich. The orientation attained using the magic angle insert was determined by a comparison with orientation obtained by a goniometer probe. For studies using the probe, the stacks were placed directly (i.e., without the insert) into a NMR tube and a goniometer probe was used to adjust the angle θ between the normal to the surface of the bilayers supports and the direction of the B_0 field. Figure 2-5 shows two set of frequency-domain spectra comparing one from a multibilayer which was oriented as close as possible to the magic angle using a goniometer probe (Fig. 2-5A) with one from a multibilayer oriented by the magic angle insert (Fig. 2-5B). ^{1}H NMR spectra in Figure 2-5 were obtained using the standard Hahn echo sequence with different separations (τ) between $\pi/2$ and π radiofrequency pulses. Under the measurement conditions of this sequence, the signal amplitude is reduced due to T_2 NMR relaxation by a factor of exp(-$2\tau/ T_2$). Hence, dependence of the signal amplitude on τ allows for the evaluation of the characteristic values of T_2, which are mostly determined by the degree of deviation from the magic angle orientation. The spectra in Figure 2-5 show partially overlapping lines of the CH_2 groups of the hydrocarbon chains and of the CH_3 choline groups of the

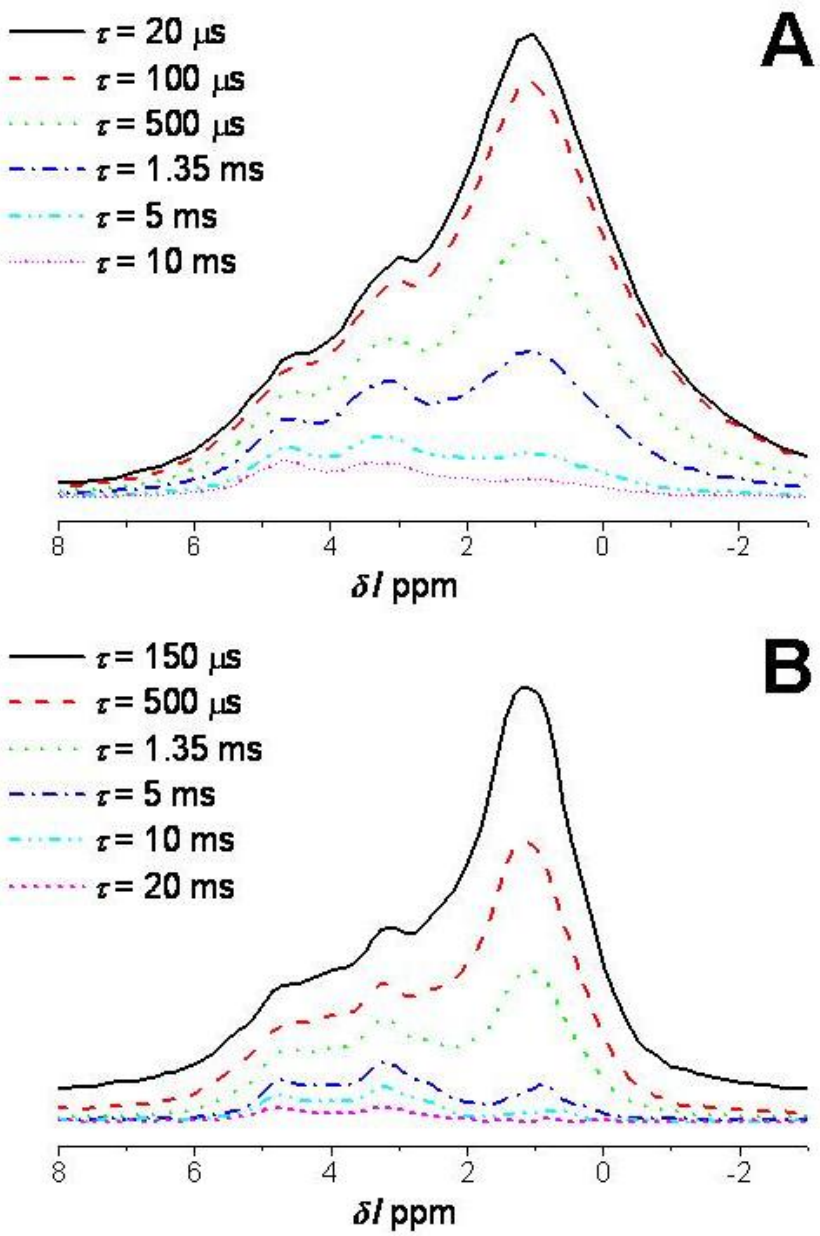

Figure 2-5. ^{1}H NMR spectra of DOPC/SM/Chol multibilayer stacks to study the macroscopic orientation of the stack using the magic angle insert. These spectra were recorded using the Hahn echo sequence for different value of τ, the duration between the first and second radiofrequency pulse, at 298 K. The stacks were aligned at the magic angle using a goniometer probe (A) and the specially designed insert shown in Fig. 2-3 (B). These data were obtained by Konstantin Ulrich. The insert has been adapted for high-field, high gradient PFG NMR studies and the new insert yields similar orientational efficiency.

headgroup at around 1 and 3 ppm, respectively. These lines can be assigned to both DOPC and SM. A line at around 4.7 ppm is assigned to a small amount of normal water. It is seen that the spectra in Figure 2-5A and their dependence on τ essentially coincide with those in Figure 2-5B. The data in Figure 2-5A were recording using a goniometer probe, which gives magic angle orientation with precision of around 0.3º. On the basis of comparison of these data with those in Figure 2-5B, it was concluded that the specially designed magic angle insert allows for the achievement of magic angle orientation with similar precision. The magic angle insert developed by Konstantin Ulrich for studies of lateral diffusion of lipids in multibilayer stacks was adapted to the relevant studies of lateral diffusion with high-field, high gradient PFG NMR. The new inserts are expected to function with similar precision.

Magnetic Susceptibility

Magnetic susceptibility can produce disturbing effects in our measurements. These effects are intensified as the strength of the magnetic field is increased. With the application of a strong external magnetic field B_0, the susceptibility difference in the PFG NMR samples can yield additional magnetic field gradients, which are expected to be stronger for larger B_0 values. Similar diffusion experiments were conducted on multibilayer stacks of lipids at three different B_0 strengths to verify the absence of such artifacts under our measurement conditions. Figure 2-6 shows examples of ^{1}H PFG NMR attenuation curves measured at different field strengths by the PFG NMR stimulated echo sequence for similar effective diffusion times and similar high and low temperatures. The effective diffusion time (t_{eff}) and sample temperature were kept constant for the measurement of each curve. These studies were used to observe

diffusion in a common ternary bilayer (DOPC/SM/Chol) under conditions where the system is expected to be compositionally homogeneous (T > 298K) and heterogeneous (T < 298 K). The details of diffusion results will be discussed in detail in Chapter 3. This section uses the results presented in Fig. 2-6 to confirm that magnetic susceptibility does not influence the data by comparing results obtained at different applied magnetic field strengths. The data in Figure 2-6 were obtained using the NMR spectrometers operating at a proton resonance frequency of 750 and 400 MHz. For each attenuation curve, the initial, *i.e.*, smallest gradient strength, was chosen in such a way that it was sufficiently small to ensure that there is no attenuation of the lipid signal and, at the same time, sufficiently high for suppression of any significant contribution of water to the measured signal. Such water suppression is possible because the diffusivity of water in the lateral direction is around 2 orders of magnitude larger than that of lipids. As a result, even an application of relatively small gradients results in vanishing of the water signal under our experimental conditions. Suppression of the water signal is especially important for the measurements using the amplitude of the time-domain signal (see solid and empty circles in Figure 2-6). For measurements at 400 MHz, the amplitude of the signal of time-domains spectra were recorded and used to plot attenuation curves. Because of this method of processing, contributions of water and lipids to this time-domain signal cannot be readily distinguished as it can be done on the basis of chemical shift difference. It is seen that the data in Figure 2-6, which were obtained at different B_0 strengths and for different types of data processing, i.e., processing of either frequency-domain or time-domain spectra, show qualitatively and quantitatively similar behavior. Results from the fits of these types of attenuation plots also give similar

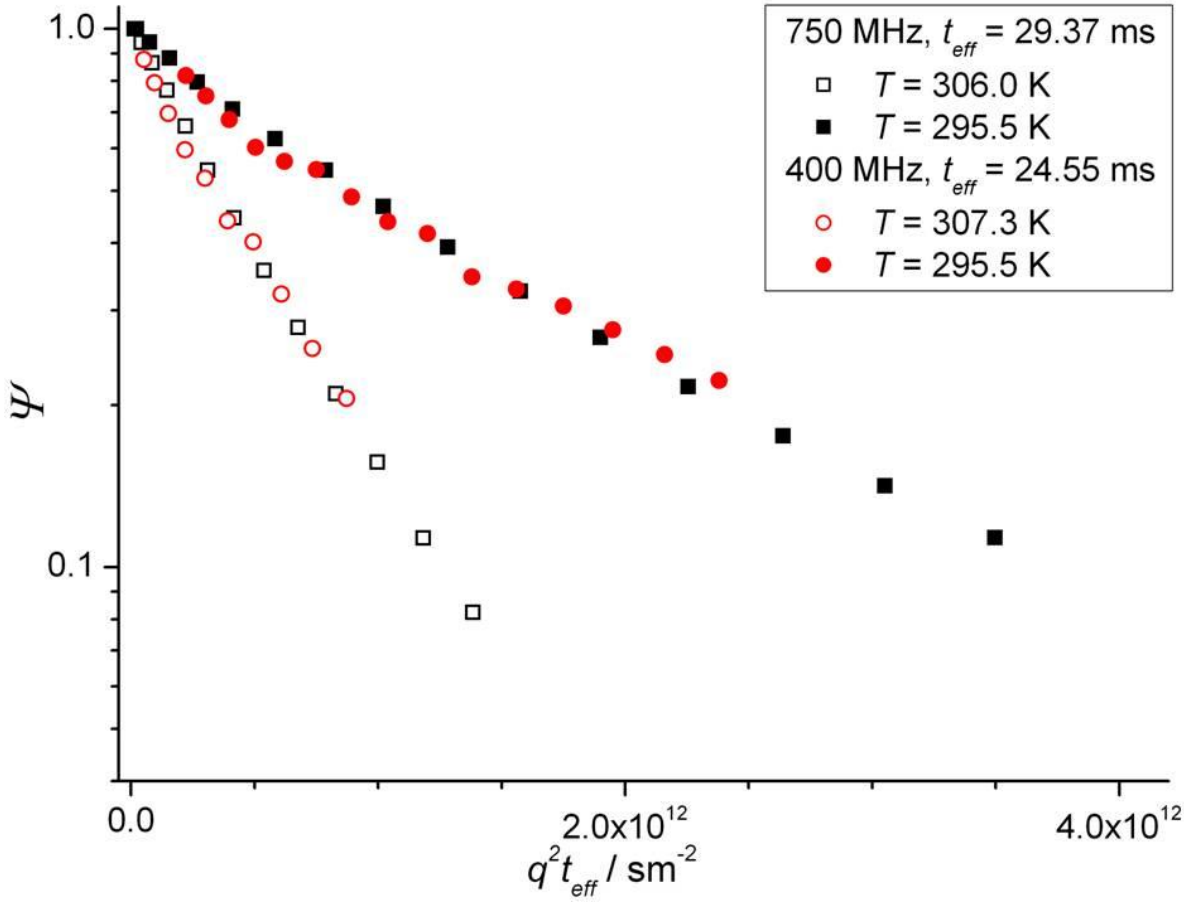

Figure 2-6. Examples of attenuation curves at different applied magnetic field strength to check for magnetic susceptibility. The attenuation data was obtained by the PFG NMR stimulated echo sequence under the following conditions: (squares) the ^{1}H resonance frequency is equal to 750 MHz and δ = 1.89 ms and (circles) the ^{1}H resonance frequency is equal to 400 MHz and δ = 1.35 ms.

diffusion behavior. This implies that there is essentially no influence of the B_0 strength on the diffusion data. This observation is important in view of the possibility that our PFG NMR diffusion data could be distorted due to difference between the magnetic susceptibility of the glass plates, bilayers stacks, insert, and the gas phase in the PFG NMR samples. The existence of large susceptibility-induced gradients would inevitably interfere with our PFG NMR measurements. However, the results in Figure 2-6 show

no evidence for such susceptibility effects because the diffusion data remain essentially the same for different B_0 values used in this work. The PFG NMR 13-interval sequence has also been used to obtain diffusion data for this type of sample. This sequence uses bipolar (alternating) pulsed-field gradients in order to suppress susceptibility-induced artifacts in diffusion experiments. The comparison of results (not shown) obtained using the PFG NMR 13-interval and STE sequences did not show any difference between results. Due to the coincidence in data at different B_0 field strengths as well as the coincidence between data obtained with these two sequences, we can conclude that under our experimental conditions the disturbing influence of the susceptibility effects on the diffusion data is negligibly small. It is also important to note the improvement in signal obtained at the high-field. Low signal-to-noise at 400 MHz causes a significant amount of scatter in the data that is essentially eliminated with the increase in field strength to 750 MHz.

CHAPTER 3
DIFFUSION AND LIPID EXCHANGE INSIDE AND BETWEEN LIPID MEMBRANE DOMAINS

Studies of Lipid Bilayers with Large Liquid-Ordered Domains

The main purpose for studies of lateral diffusion in bilayers consisting of a ternary mixture of DOPC, sphingomyelin, and cholesterol was to demonstrate that it is feasible to adapt the PFG NMR technique using high-field (17.6 T) and high-gradients strengths (up to 30 T/m) for studies of lateral diffusion in model membranes. Diffusion and structural studies of bilayers and vesicles formed from equimolar mixtures of DOPC/SM/CHOL have been reported extensively in the literature which gives an appropriate comparison for the verification of the new technique.[31,35,90] Application of high-field NMR allows for measurements of samples with superior signal-to-noise ratio which can be crucial when collecting data from samples that have relatively weak NMR signal such as that of lipids in bilayers. The ratio of signal-to-noise is expected to increase with increasing applied field strength according to NMR theory. All data from this point on was collected at a high field of 17.6 T corresponding to a proton frequency of 750 MHz. Application of high gradients allows for the use of sufficiently short diffusion times under the conditions of the narrow-pulse approximation, which requires that the gradient duration is small in comparison to the diffusion time. Short diffusion times correspond to short observed displacements. As a result, application of strong gradients leads to the possibility of diffusion measurements over a wide range of length scales including submicrometer length scales. The following discussion presents results of diffusion studies for the case in which domains are much larger than the experimentally measured lipid displacements. In membranes composed of a ternary

mixture of DOPC/SM/Chol, domains have been observed to be as large as 10 μm.[31,35] The largest displacement probed is on the order of 1μm. In this case, diffusion behavior is independent of diffusion time.

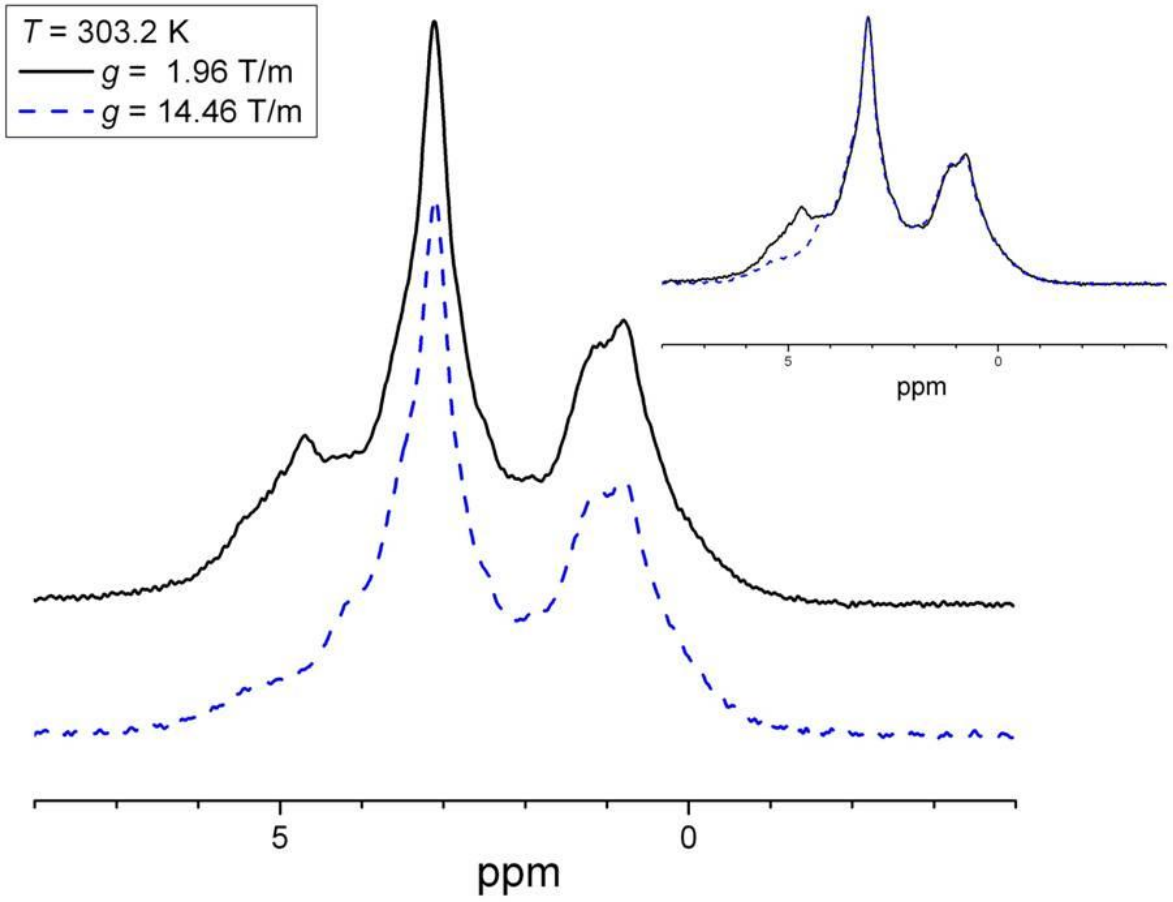

Figure 3-1. ^{1}H NMR spectra of DOPC/SM/Chol multibilayer stacks measured by the PFG NMR stimulated echo sequence at 750 MHz for different values of the gradient amplitude (g) at T = 303.2 K. The inset shows the spectra obtained using the larger gradient strength scaled such that the intensities of the CH_3 lines match.

Figure 3-1 shows examples of ^{1}H NMR spectra of the oriented multibilayer stacks of DOPC/SM/Chol measured by the stimulated echo PFG NMR sequence at 303.2 K under the measurement conditions used for diffusion studies at high-field and high-gradient strengths. The spectra are from measurements at an initial gradient strength of

1.96 T/m (solid) and an intermediate gradient strength of 14.46 (dashed). The spectra in Figure 3-1 show that under the measurement conditions at 750 MHz the spectral resolution allows distinguishing the NMR lines corresponding to CH_3, CH_2, and H_2O. Each spectrum shows partially overlapping lines of the CH_2 groups of the hydrocarbon chains and of the CH_3 groups of the lipid headgroups at around 1 and 3 ppm, respectively. This signal originates from the phospholipids. No signal from CHOL can be observed due to the short T_2 NMR relaxation times of this rigid molecule.[90] A line at around 4.7 ppm is assigned to a small amount of normal water present in the sample. The smallest gradient strength (*i.e.*, 1.96 T/m) was chosen in such a way that it was sufficiently small to ensure that there is no attenuation of the lipid signal and at the same time, sufficiently high for suppression of any significant contribution of water to the measured signal. The spectra were obtained at *a* temperature well above the miscibility transition temperature, T_m, for this sample. Above the T_m, the bilayer is expected to be one homogeneous phase with a single lipid diffusivity. The inset of Fig. 3-3A presents the two spectra superimposed where the spectrum obtained using the intermediate gradient strength is scaled such that the intensities of the CH_3 signals are equivalent. The coincidence in signal shape of the two spectra is nearly exact except for a small difference corresponding to the loss of the water line. This change is minor and does not significantly affect the measurement of lipid self-diffusion. Figure 3-2 shows the examples of ^1H PFG NMR attenuation curves. The attenuation data was measured by the PFG NMR stimulated echo sequence for different effective diffusion times at high and low temperatures at 750 MHz. During the measurement of each curve, these

parameters (t_{eff} and T) were kept constant and the initial, *i.e.*, smallest gradient strength, was chosen to be sufficiently small to ensure that there is no attenuation of the lipid

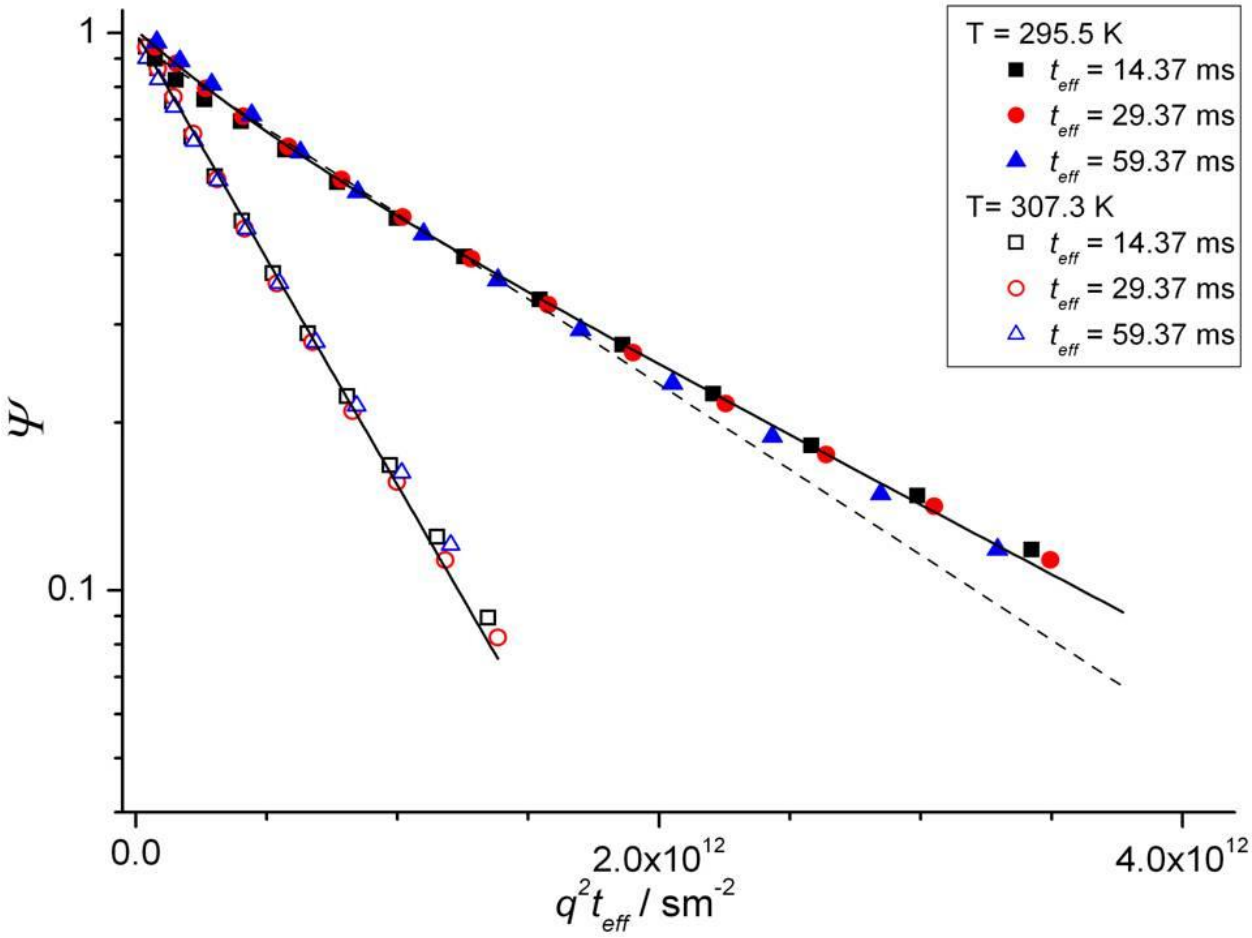

Figure 3-2. PFG NMR attenuation curves for DOPC/SM/Chol samples obtained at three diffusion times at low and high temperature at 750 MHz. At high temperatures, *i.e.*, T > 298.2 K, the bilayers are expected to be homogeneous. At temperatures below 298.2 K, liquid-ordered domains are expected to form. Analysis of the data shows that at the high temperature, there is a single ensemble of lipids with one diffusion coefficient. To the contrary, at low temperatures there are two ensembles of lipids diffusing with different diffusivities. These two ensembles correspond to lipids diffusing inside and outside of liquid-ordered domains. These domains are large in comparison to the length scales of lipid displacements probed in the experiments.

signal and, at the same time, sufficiently high for suppression of any significant contribution of water to the measured signal. In the presentation of Figure 3-2, the

attenuation curves obtained for different diffusion times are expected to coincide if the diffusivity(ies) of the probed lipids remain the same with increasing or decreasing diffusion time and the corresponding values of the mean square displacement. The data in this figure indicate that there is essentially no dependence of the attenuation curves and of the corresponding diffusion behavior on diffusion time. Such results were obtained for all measured temperatures. Fitting attenuation curves by Eq. 18 has shown that for temperatures lower than T = 298 K, the two-exponential fit (Eq. 18 with n = 2, solid line) produces better results than the one-exponential fit (Eq. 18 with n = 1, dashed line). At the same, time for temperatures higher than T = 298 K, it has been sufficient to use the single-exponential curves (solid line) to fit the experimental data satisfactorily (Fig. 3-2). In the latter case, the two-exponential fit either produced two diffusivities, which were identical within the uncertainty of the fitting procedure, or it gave an extremely small value (several percent) for one of the fractions, which was comparable to the fitting error. T = 298 K corresponds to the transition temperature for the liquid-disordered-liquid-ordered phase coexistence, $T_{m.}$ Above this temperature, the bilayer is expected to be structurally homogeneous, *i.e.*, no domains are formed. Monoexponential behavior corresponds to a single diffusivity for all lipids contributing to the measured signal (*i.e.*, DOPC and SM).

Figure 3-3 shows an Arrhenius-type plot of the temperature dependence of diffusivities, which result from fitting the attenuation curves for different values of the constant magnetic field. There is agreement between diffusion data collected at the three B_0 field strengths. Scatter in the diffusivity values at temperatures $T < T_m$ when two-exponential fit of the attenuation curves becomes necessary is mostly associated

with signal-to-noise limitations of measurements at the two lower proton resonance frequencies (see Fig. 2-6). These limitations are especially pronounced at large signal

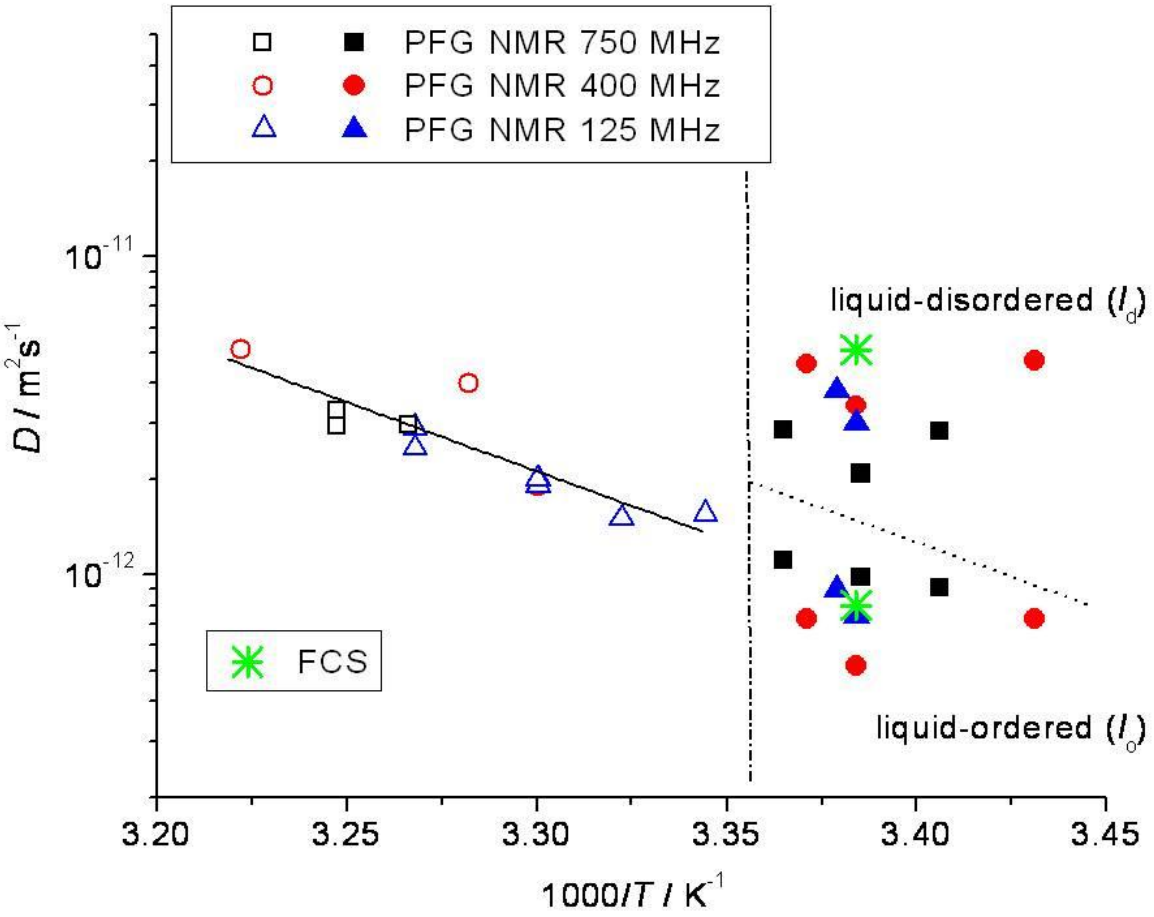

Figure 3-3. Lateral diffusivities of lipids in DOPC/SM/Chol multibilayer stacks plotted as a function of inverse temperature. Diffusivities are obtained from two-exponential fit (filled symbols) and monoexponential fit (empty symbols) of PFG NMR attenuation curves measured at a proton resonance frequency of 125, 400, and 750 MHz. Also shown for comparison are diffusion coefficients (*) recorded by fluorescence correlation spectroscopy (FCS) in lipid membranes with the same composition (from ref 89). The solid line shows the best fit of the diffusivities measured at $T > T_m$ using the Arrhenius law $\{D = D_0 \exp[-E_a / RT]\}$ with E_a = 91kJ/mol.

attenuation corresponding to diffusion in the liquid-ordered phase. In comparison, the signal-to-noise ratio of the ^{1}H PFG NMR measurements at 750 MHz was appreciably

better. It is important to note that no systematic changes in the measured diffusivities were observed with increasing proton frequency. The results in Figure 3-3 were obtained with several different bilayer samples prepared in two different countries. Hence, under these circumstances, the agreement between the data in the figures can be considered to be satisfactory. Under these measurement conditions, the characteristic sizes of liquid-ordered domains are expected to be in the range of much greater than 1 micron (*i.e.,* much larger than the root-mean-square displacements of lipids (Eq. 5) for all effective diffusion times used). Hence, the possible influence of diffusion restrictions by the domain boundaries and of molecular exchange between different domains on the measured diffusivities can be ruled out. This conclusion is in agreement with the observations that the diffusivities measured at each temperature do not depend on diffusion time. The values of diffusivities obtained by PFG NMR with high field and high gradient strengths in this section are in good agreement with those obtained using FCS[31] and PFG NMR with conventional gradient strenghts[90] in lipid membranes with the same or similar composition. This is demonstrated by the comparison of data from PFG NMR studies at high-field and high-gradient strengths and the previously reported FCS results in Figure 3-2.

Observation of Lipid Exchange Between Domains and Their Surroundings in Lipid Bilayers with Small Liquid-Ordered Domains for Exchange Studies

Domains on the order of 1 μm or smaller, which is significantly smaller than those reported for other systems such as DOPC/SM/Chol discussed in the previous section, have been observed for model lipid membranes composed of a ternary mixture of DOPC/DPPC/Chol.[29,46] Smaller domains are often considered to be a better representation of lipid rafts and can be used to obtain new fundamental information

about lipid dynamics in cell membranes. It is important to note that in comparison with the previous studies, PFG NMR at high-field and high-gradient strengths allows for the characterization of diffusion behavior under conditions of the narrow-pulse approximation on a length scale as small as 100 nm, *i.e.*, a much smaller length scale than in the previous similar measurements. The technique is then quite attractive for those interested in studying diffusion restrictions and inter-domain exchange which can become significant in small domains (≤1 μm). Diffusion restrictions can be caused by the presence of transport barriers at the domain boundaries. High-field, high-gradient PFG NMR studies of time-dependent diffusion behavior can give qualitative and quantitative information about the size of the domains, molecular exchange between domains and the surrounding disordered environment, and the permeability of the domain boundaries.

Figure 3-4 shows examples of ^{1}H NMR spectra of the oriented stacks of bilayers measured by the stimulated echo PFG NMR sequence under the measurement conditions used for diffusion studies at high-field and high-gradient strengths. Both Figure 3-4A and 3-4B show spectra from measurements at an initial gradient strength (solid) and an intermediate gradient strength (dashed). Much like Fig. 3-1, each spectrum shows partially overlapping lines of the CH_2 groups of the hydrocarbon chains, the CH_3 groups of the lipid headgroups, and the normal water at around 1, 3 and 4.7 ppm, respectively. The smallest gradient strength (*i.e.*, 0.33 T/m) was chosen in such a way that it was large enough to suppress most of the water signal but sufficiently small so that there was no attenuation of lipid signal at that gradient amplitude.

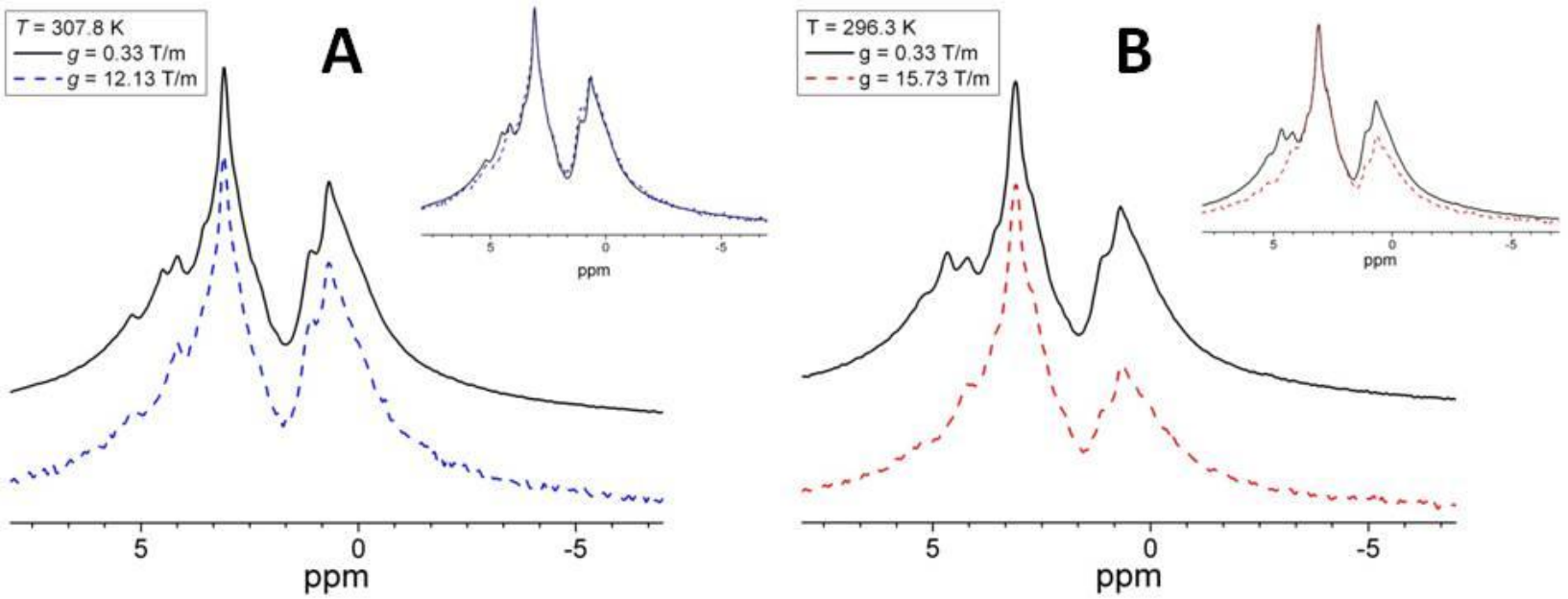

Figure 3-4. ^{1}H NMR spectra of DOPC/DPPC/Chol multibilayer stacks measured by the PFG NMR stimulated echo sequence for different values of the gradient amplitude (*g*) at *T* = 307.8 K (A) and *T* = 296.3 K (B) at 750 MHz. For each set of spectra, the inset shows the spectra obtained using the larger gradient strength scaled such that the intensities of the CH_3 lines match.

Figure 3-4A shows spectra obtained at T = 307.8 K, a temperature well above the miscibility transition temperature, T_m, for this sample, at gradient amplitudes of 0.33 and 12.13 T/m. The inset of Fig. 3-4A presents the two spectra superimposed where the spectrum obtained using the intermediate gradient strength is scaled such that the intensities of the CH_3 signals are equivalent. The superposition of spectra shows the same coincidence in shape of spectra as in Fig. 3-1 which would be expected for a homogeneous bilayer.

Figure 3-4B shows spectra obtained at T = 296.3 K using gradient amplitudes of 0.33 and 15.73 T/m. The intermediate gradient strengths at each temperature correspond to approximately the same attenuation of signal. At lower temperatures, the diffusivities of lipids are smaller requiring larger gradient amplitudes to reach the same level of attenuation as that at higher temperatures. In the inset of Figure 3-4B, the two spectra are shown with the spectrum obtained using the intermediate gradient strength scaled such that the intensities of the CH_3 signals are equivalent. Unlike Fig. 3-4A, the spectra show that the shapes of the NMR spectra depend on the applied gradient strength. The line corresponding to the CH_2 groups appears to attenuate at a larger rate than the line for the CH_3 groups. This occurs because each spectrum obtained at this temperature is a superposition of signals coming from two components, a slow and a fast diffusion component[90] corresponding to diffusion inside the l_o and l_d phases, respectively.[46,88] The l_o domains are enriched in DPPC and characterized by a tighter packing and lower diffusivity of lipids in comparison to the DOPC-enriched l_d phase. The NMR lines of CH_2 and CH_3 groups shown in Fig. 3-4B have different contributions from both phases. The change in shapes of the spectra that is seen in Fig. 3-4B is a

consequence of a larger decrease of the contribution from the phase with the highest diffusivity, *i.e.*, l_d phase, with increasing gradient strength. The spectra in Fig. 3-4 show that in all cases the amplitude of the choline CH_3 line is larger than the amplitude of the CH_2 line despite the fact that fewer protons contribute to the former line than to the latter. This results from the influence of T_2 NMR relaxation.[90] Under the measurements conditions of the PFG NMR stimulated echo sequence, signal amplitude is reduced due to T_2 NMR relaxation by a factor, $\exp(-2\tau/T_2)$. As already mentioned above, in lipid bilayers the rate of T_2 NMR relaxation is enhanced by proton dipole-dipole interactions. Protons in the hydrocarbon chains of lipids are expected to have shorter T_2 NMR relaxation times in the l_o phase than in the l_d phase due to increased packing order in the former phase.[88] In comparison to protons in the hydrocarbon chains, protons in the headgroups of lipids residing in both l_o and l_d phases have a higher flexibility with respect to reorientations. Hence, T_2 times of these protons are less sensitive to dipole-dipole interactions resulting in larger T_2 values. T_2 NMR relaxation times were estimated by performing a series of STE experiments with $g \approx 0$ T/m and varying the value of τ_1, the time between the first two $\pi/2$ pulses. These values were found to be on the order of ~ 6 ms and ~12 ms, for CH_2 and CH_3, respectively. Therefore the choline CH_3 line is used for obtaining diffusion data at all temperatures. For selected experiments, the data was treated using the amplitudes of the CH_2 line in the attenuation plots in order to verify that diffusion coefficients, which were obtained from fitting the data by Eq. 18 would agree with the corresponding data obtained using the CH_3 line. The only difference between the treatment of the two lines is the phase fractions obtained since the measured signal of the l_o phase is more significantly

reduced by T_2. While signal amplitude is reduced for both lines, the CH_3 line is a better representative of the signal unperturbed by the T_2 NMR relaxation process.

Diffusion Results

Figure 3-5 shows examples of ^{1}H PFG NMR attenuation curves measured by the PFG NMR stimulated echo sequence for different effective diffusion times at five different temperatures at a proton frequency of 750 MHz. Fitting the attenuation curves in Fig. 3-5A by Eq. 18 has shown that for T = 307.8 K, it is sufficient to use the one-exponential curve (Eq. 18 with n = 1) in order to fit the experimental data satisfactorily. Single-exponential behavior corresponds to a single diffusivity for all lipids contributing to the measured signal. In the presentation of Fig. 3-5, the curves obtained for different diffusion time are expected to coincide if the diffusivity of the probed lipids remains the same with increasing or decreasing diffusion time and the corresponding values for mean square displacement. The data in this Fig. 3-5A indicate that there is no dependence of the attenuation curves and of the corresponding diffusion behavior on diffusion time at 307.8 K. Hence, it can be concluded that all probed lipids diffuse with the same diffusivity, which is independent of diffusion time in the measured range.

Figure 3-5A displays one curve obtained by a sequence known as the PFG NMR stimulated echo longitudinal-encode-decode sequence (STE LED) measured with t_{eff} = 4.24 ms. In comparison to the traditional PFG NMR STE sequence, this sequence has an additional delay before the data acquisition to allow for a decay of eddy currents.[114] It is possible not only to compare results obtained using the PFG NMR STE and STE LED sequences to check for influence of eddy currents but also to obtain results using much smaller effective diffusion time (as low as 4.24 ms). In measurements with the former sequence, all essential parameters such as the total duration of the gradient

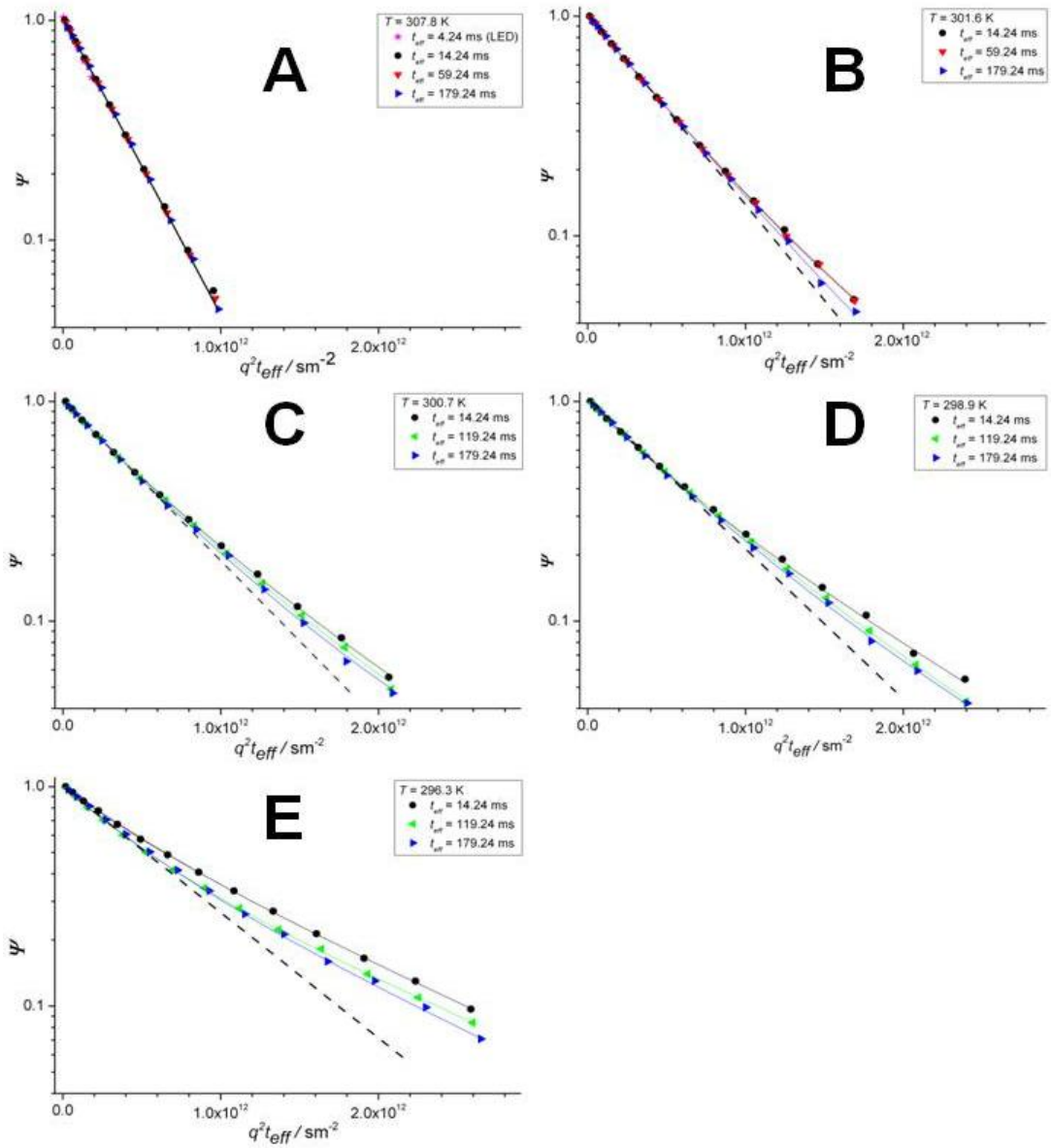

Figure 3-5. Examples of diffusion attenuation curves obtained for DOPC/DPPC/Chol by the PFG NMR stimulated echo sequence at T = 307.8 K (A), T = 301.3 K (B), T = 300.7 K (C), T = 298.8 K (D), and T = 296.3 K (E) at 750 MHz. All attenuation curves were obtained by measuring the intensity of the choline spectra. In part A, the solid line is a single-exponential fit of all data in the figure. In parts B-E, solid lines are individual two-exponential fits of each curve using Eq. 18 with n = 2. The dashed lines show monoexponential curves corresponding to the initial decay of the measured attenuation curves.

pulse, effective diffusion time, and temperature were kept the same or similar as in the measurements with the later sequence. As expected, no significant changes in the initial slope of attenuation curves (not shown) or the related effective diffusivity were observed when using the PFG NMR STE LED sequence.

Figure 3-5E is a collection of attenuation curves similar to that shown in Fig. 3-5A for experiments conducted at 296.3 K, a temperature well below the T_m for this mixture. These curves show pronounced deviations from the monoexponential behavior prescribed by Eq. 18 with n = 1 (dashed line). At the same time, fitting the attenuation curves by Eq. 18 with n = 2 produces satisfactory results (solid lines). This biexponential behavior indicates the existence of two ensembles of lipids with different diffusion coefficients. The smaller diffusion coefficient can be assigned to the l_o phase and the larger diffusion coefficient to the l_d phase. For any particular phase, the diffusivities of all lipid species present in that phase in multi-component bilayers can be expected to be essentially the same or similar on the basis of the results of previous experimental studies.[87,115] This expectation is also confirmed by the data in Fig. 3-5A showing that the diffusion behavior is the same for all lipids contributing to the measured choline signal (*i.e.*, DOPC and DPPC).

Figures 3-5B, 3-5C, and 3-5D show qualitatively similar attenuation curves measured at 301.6, 300.7, and 298.9 K, respectively. As in Fig. 3-5E, there is deviation from a single-exponential fit of the initial slope (dashed lines) indicating that a two-exponential fit using Eq. 18 with n = 2 (solid lines) provides a more appropriate description of the measured data. As the temperature approaches the T_m for this mixture, the extent of deviation from the single-exponential behavior becomes smaller

Table 3-1. Results from fitting of the PFG NMR attenuation curves of DOPC/DPPC/Chol at different temperatures as seen in Figure 3-5 by Eq. 18.

T = 307.8 K				
t_{eff} ms	p_o	$D_o\times10^{12}$ m^2/s	p_d	$D_d\times10^{12}$ m^2/s
8.24	-	-	1	4.7 ± 0.5
14.24	-	-	1	4.7 ± 0.5
29.24	-	-	1	4.7 ± 0.5
59.24	-	-	1	4.6 ± 0.5
179.24	-	-	1	4.5 ± 0.4
T = 301.6 K				
t_{eff} ms	p_o	$D_o\times10^{12}$ m^2/s	p_d	$D_d\times10^{12}$ m^2/s
8.24	0. 24± 0.07	1.6 ± 0.2	0.76 ± 0.08	3.5 ± 0.3
14.24	0.19 ± 0.08	1.6 ± 0.2	0.81 ± 0.08	3.3 ± 0.3
29.24	0.14 ± 0.03	1.4 ± 0.1	0.87 ± 0.09	3.2 ± 0.3
59.24	0.11 ± 0.04	1.3 ± 0.3	0.89 ± 0.09	3.1 ± 0.3
179.24	0.02 ± 0.02	1.0 ± 0.4	0.97 ± 0.10	2.9 ± 0.3
T = 300.7 K				
t_{eff} ms	p_o	$D_o\times10^{12}$ m^2/s	p_d	$D_d\times10^{12}$ m^2/s
8.24	0.69 ± 0.11	1.8 ± 0.2	0.31 ± 0.11	4.3 ± 0.8
14.24	0.62 ± 0.12	1.8 ± 0.2	0.38 ± 0.12	4.2 ± 0.8
29.24	0.52 ± 0.18	1.6 ± 0.2	0.48 ± 0.18	3.8 ± 0.7
59.24	0.41 ± 0.14	1.5 ± 0.2	0.59 ± 0.14	3.3 ± 0.5
179.24	0.21 ± 0.15	1.2 ± 0.5	0.79 ± 0.15	2.8 ± 0.3
239.24	0.17 ± 0.12	1.1 ± 0.4	0.83 ± 0.12	2.8 ± 0.3
T = 298.9 K				
t_{eff} ms	p_o	$D_o\times10^{12}$ m^2/s	p_d	$D_d\times10^{12}$ m^2/s
8.24	0.73 ± 0.07	1.7 ± 0.2	0.27 ± 0.03	4.1 ± 0.4
14.24	0.61 ± 0.08	1.6 ± 0.2	0.39 ± 0.08	3.6 ± 0.6
59.24	0.49 ± 0.05	1.5 ± 0.2	0.49 ± 0.05	3.4 ± 0.3
179.24	0.18 ± 0.08	1.1 ± 0.2	0.82 ± 0.08	2.6 ± 0.3
239.24	0.15 ± 0.09	1.1 ± 0.2	0.85 ± 0.09	2.7 ± 0.3
T = 296.3 K				
t_{eff} ms	p_o	$D_o\times10^{12}$ m^2/s	p_d	$D_d\times10^{12}$ m^2/s
14.24	0.70 ± 0.07	1.2 ± 0.1	0.30 ± 0.03	4.0 ± 0.7
29.24	0.63 ± 0.06	1.1 ± 0.1	0.37 ± 0.04	3.7 ± 0.4
59.24	0.57 ± 0.06	1.1 ± 0.1	0.43 ± 0.06	3.1 ± 0.3
119.24	0.53 ± 0.05	1.1 ± 0.1	0.47 ± 0.05	3.3 ± 0.3
179.24	0.44 ± 0.09	1.0 ± 0.1	0.56 ± 0.09	2.8 ± 0.3
239.24	0.42 ± 0.04	1.0 ± 0.1	0.58 ± 0.06	3.1 ± 0.3

(compare solid and dashed lines). This change could be a consequence of a change of diffusion coefficients, phase fractions, or a combination of the two. There is also a noticeable change in diffusion behavior with increasing effective diffusion time. Table 3-1 reports the best fit results for the curves in Fig. 3-5, *i.e.*, diffusivities and the corresponding fractions in l_o and l_d phases. The error of data in the table has contributions from a number of sources including uncertainties associated with the calibration of gradient strength, sample preparation, the reproducibility of the measured PFG NMR attenuation curves, and the fitting of data using Eq. 18. For most measurements, the total error did not exceed ±10%. In some cases, the reported uncertainty was larger than ±10% due to a larger error associated with fitting the data by Eq. 18.

Time-Dependent Diffusion Behavior

One very significant characteristic of the data in Figure 3-5 is the manner in which diffusion behavior changes with effective diffusion time at temperature below T_m (see Fig. 3-5B thru 3-5E). Effective diffusion times are directly related to the root-mean square displacements of lipids according to the Einstein relation $\sqrt{\langle r^2(t)\rangle} = \sqrt{4Dt_{eff}}$ for two-dimensional diffusion. Hence, the observed changes in the diffusion behavior can be directly attributed to the changes in the lipid displacements. If the domains are much larger than the lipid displacements during the experimental observation time (t_{eff}) or do not exist at all, the PFG NMR attenuation curve for different t_{eff} values are expected to coincide with each other and give the same values of diffusivity within experimental error (see Fig. 3-5A). In the case that the size of domains is comparable to the lipid

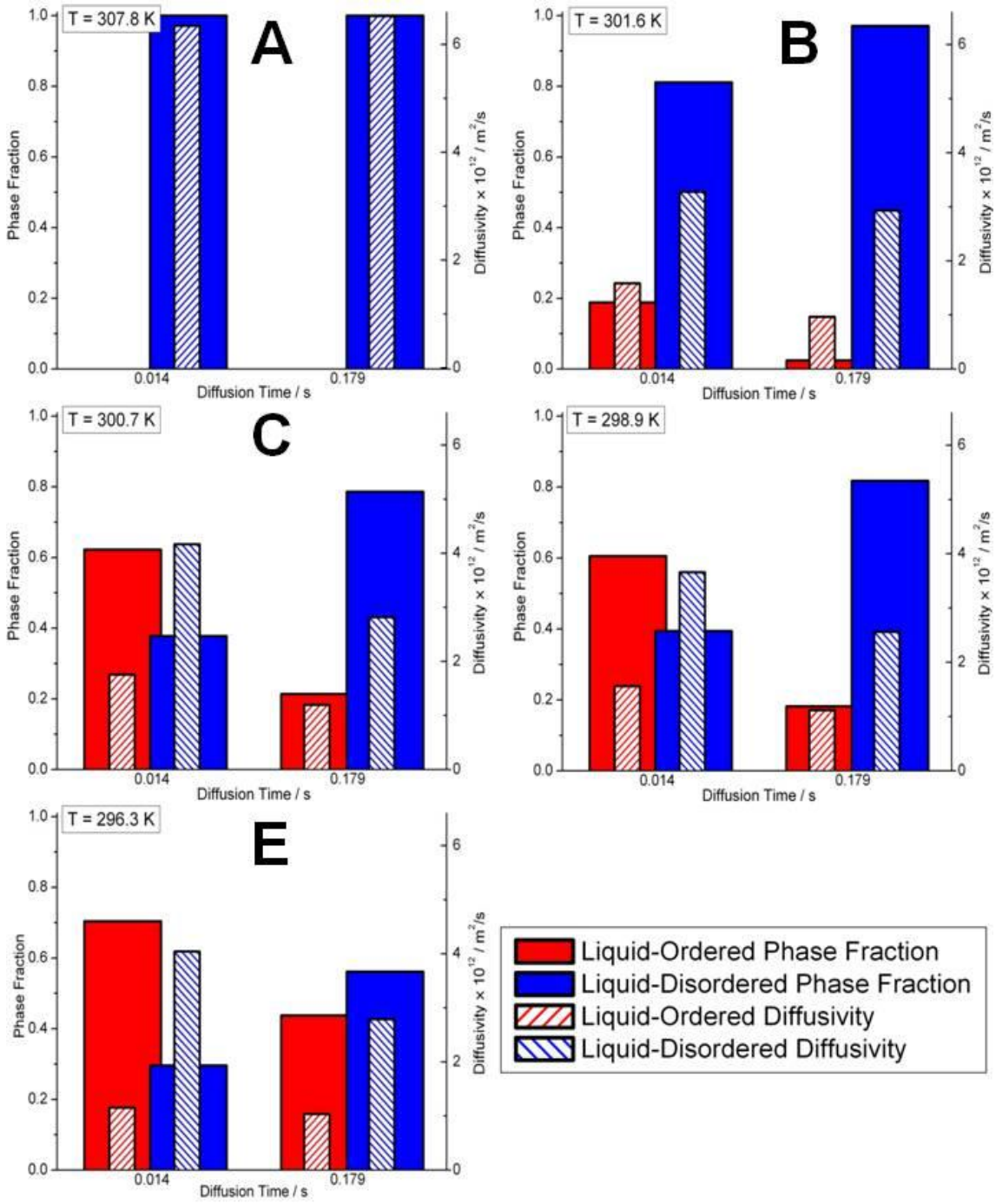

Figure 3-6. Comparison of diffusion behavior at different effective diffusion times for experiments conducted on DOPC/DPPC/Chol at T = 307.8 K (A), T = 301.6 (B), T = 300.7 (C), T = 298.9 K (D), and T = 296.3 K (E). The amplitudes of the columns show the phase fractions (left vertical axis) of the l_o (red) and l_d (blue) phases while the amplitude of the striped columns correspond to the diffusivities (right vertical axis) of the phases of solid columns on which they are superimposed.

displacements, diffusion behavior is expected be dependent on the effective diffusion time.[116]

Figure 3-6 illustrates diffusion behavior at small (14.24 ms) and large (179.24 ms) values of t_{eff} for each temperature (below T_m) reported in Fig. 3-5. In each case, the fraction of molecules attributed to the diffusion inside l_o domains decreases with an increase in t_{eff} which indicates an existence of exchange between the l_o and l_d phases. The data in Fig. 3-6 indicate that at the larger t_{eff}, most lipids diffuse either in the l_d phase or diffuse a fraction of the diffusion time in the l_o domains and the remaining fraction of diffusion time in the l_d phase. The diffusivity values of lipids in the l_d phase is ~2-3 times larger than that for the l_o phase (Table 3-1). for this reason, lipids that spend even a small fraction of the observation time in the l_d phase will be attributed to the l_d phase fraction because their overall effective diffusivity will be closer to that of the l_d rather than the l_o phase. The experimental observation that with increasing t_{eff} the decrease in the fraction of lipids attributed to the l_o phase is larger at T = 301.6 K than at lower temperatures (Fig. 3-6) indicates that the extent of exchange between the two phases is greater at the former temperature.

Relaxation Effects

It is important to note that, in addition to the lipid exchange between different types of domains, the observed dependence of the diffusion behavior on diffusion time (Fig. 3-6) can be caused by an influence of the characteristic longitudinal NMR relaxation (T_1 relaxation) on the measured PFG NMR signal. Such influence can arise if the T_1 times are sufficiently short and different for the proton signal of the choline groups of lipids located in different phases. In this case, the contribution to the measured PFG NMR STE signal from lipids with smaller T_1 would decrease with increasing diffusion time

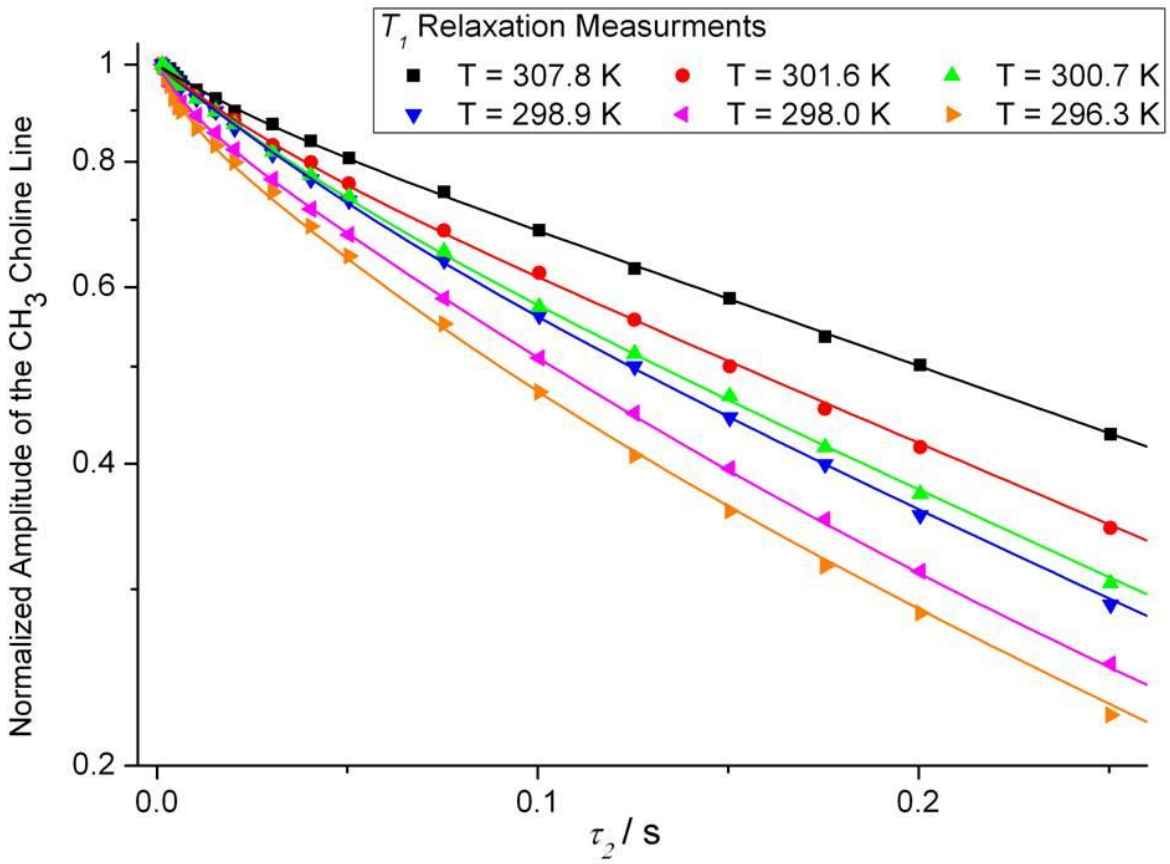

Figure 3-7. T_1 NMR relaxation curves for DOPC/DPPC/Chol bilayers obtained using the PFG NMR STE sequence with g < 1 T/m for the range of relevant temperatures. τ_2 denotes the delay between the second and third $\pi/2$ pulses of the sequence. The delay between the first and second $\pi/2$ pulses of the PFG NMR STE sequence was kept constant at 3.65 ms.

(note that $\tau_2 \approx t_{eff}$) relative to that corresponding to larger T_1. Figure 3-7 gives T_1 NMR relaxation curves measured for the line of the CH_3 choline group. The measurements were performed by the stimulated echo sequence for the same temperature range as that used in diffusion measurements. A series of one-dimensional PFG NMR STE experiments were carried out at each temperature using a gradient amplitude which was sufficiently small to ensure that there was no attenuation of the lipid signal due to diffusion but sufficiently large to suppress water signal. The delay (τ_2) between the second and third $\pi/2$ radiofrequency pulses in the sequence was varied over a range that corresponds to the range of t_{eff} values used in the PFG NMR STE diffusion measurements. During τ_2, signal amplitude is reduced by T_1 NMR relaxation by a factor, exp ($-\tau_2/T_1$). The normalized amplitude of the choline line was plotted against τ_2 along with the curve which were obtained by fitting each set of data with either a biexponential or triexponential curve. The T_1 NMR relaxation curves show non-monoexponential behavior at all temperatures including the highest temperature corresponding to the compositionally homogeneous bilayers (Fig. 3-7). For highly resolved spectra of lipid bilayers in which lines of different proton types (*i.e.*, choline, methylene, etc.) do not overlap, monoexponential T_1 curves are expected for each type of protons.[117,118] Each type of protons is capable of having unique relaxation behavior. Under our experimental conditions, the lines of the choline and methylene groups, which are expected to have different T_1 values, show a significant overlap (Fig. 3-4). Hence, the non-monoexponential behavior of the relaxation data at the highest temperature in Fig. 3-7 can be attributed to the existence of such overlap. With decreasing temperatures, the linewidth of both CH_3 choline and CH_2 groups become

broader leading to a more pronounced overlap.[117] The deviation from monoexponential behavior is therefore expected to become larger as temperature is decreased from 307.8 to 296.3 K. This expectation is in agreement with the data in Fig. 3-7. In addition to the existence of signal overlap discussed above, the non-monoexponential behavior of the T_1 plots at low temperatures can be related to the inhomogeneous nature of the lipid bilayers exhibiting the existence of l_o and l_d phases. Clearly, the T_1 NMR times for the CH_3 choline group can be different in different types of phases. The later can contribute to the observed deviations of the T_1 plots at low temperatures from the monoexponential behavior (see discussion below).

From the results in Fig. 3-7, it can be concluded that for the same t_{eff}, the influence of T_1 NMR relaxation on the measured PFG NMR signal becomes larger with decreasing temperature. This is in agreement with the results of studies showing an increase in T_1 NMR relaxation rates of lipids in the same or similar types of lipid bilayers as the temperature decreases.[69,117,118] In addition, the difference between the values of T_1 in different phases can become more pronounced at smaller temperatures. The later is related to the expectation that many properties of the l_o and l_d phases, including NMR relaxation times, become more similar as the temperature is increased to approach the T_m. In agreement with this expectation, the deviations of the T_1 NMR relaxation curves in Fig. 3-7 from the monoexponential behavior become slightly less pronounced with increasing temperature. The discussion above suggests that the influence T_1 on the t_{eff}-dependence of the fractions of lipids with different diffusivities has to be smaller at the temperatures near the T_m. At the same time, the results in Table 3-1 and Figure 3-6 show that the t_{eff}-dependence of the fractions of lipids with different diffusivities is much

stronger at larger temperatures than at smaller temperatures. Hence, we can conclude that the possible disturbing influence of T_1 NMR relaxation cannot be of large significance for the observed t_{eff} dependencies of the diffusion behavior at temperatures near the transition temperature. As a result, our experimental data at these temperature(s) can be used to obtain quantitative information on the exchange of lipids between different types of domains and on the domain properties. In particular, we have attempted to estimate the permeability of the domains boundaries for diffusing lipids as well as the sizes of l_o domains.

Extracting Quantitative Information from the Lipid Exchange Data

The discussion thus far concludes that time-dependent diffusion behavior observed for DOPC/DPPC/SM multibilayer stacks is for the most part a consequence of the lipid exchange between the liquid-ordered domains and the surrounding liquid-disordered environment. Lipid exchange occurs over times scales comparable to the experimental effective diffusion times. Accordingly, this is indicative that the sizes of the domains are comparable to the length scales of the lipid displacements during the diffusion times used. In this case, the domain boundaries can act as barriers to lateral diffusion during measurements. Time-dependent diffusion behavior studied in the presence of confining geometries can give important information about the domain itself. Mitra and colleagues[112,119-121] proposed a method which uses the short-time limit of the diffusion data recorded in the presence of transport restrictions to extract information about the spatial extensions of such restrictions. In particular, the perimeter-to-surface area of restricting two-dimensional domains can be obtained using this formulism. In this formulism, $D_{o,t\to 0}$ represents the diffusivity of molecules for the

limiting case of short diffusion times when the diffusion is not influenced by the domain boundaries. In the short-time limit, molecules only sense the presence of the domain boundaries if they are within a distance of $\left(D_{o,t\to 0}t_{eff}\right)^{1/2}$ from the walls. Those molecules represent only a small fraction of the total number of molecules in the domain. This fraction, $S\left(D_{o,t\to 0}t_{eff}\right)^{1/2}/V_p$ where S is the external surface area of the domain and V_p is

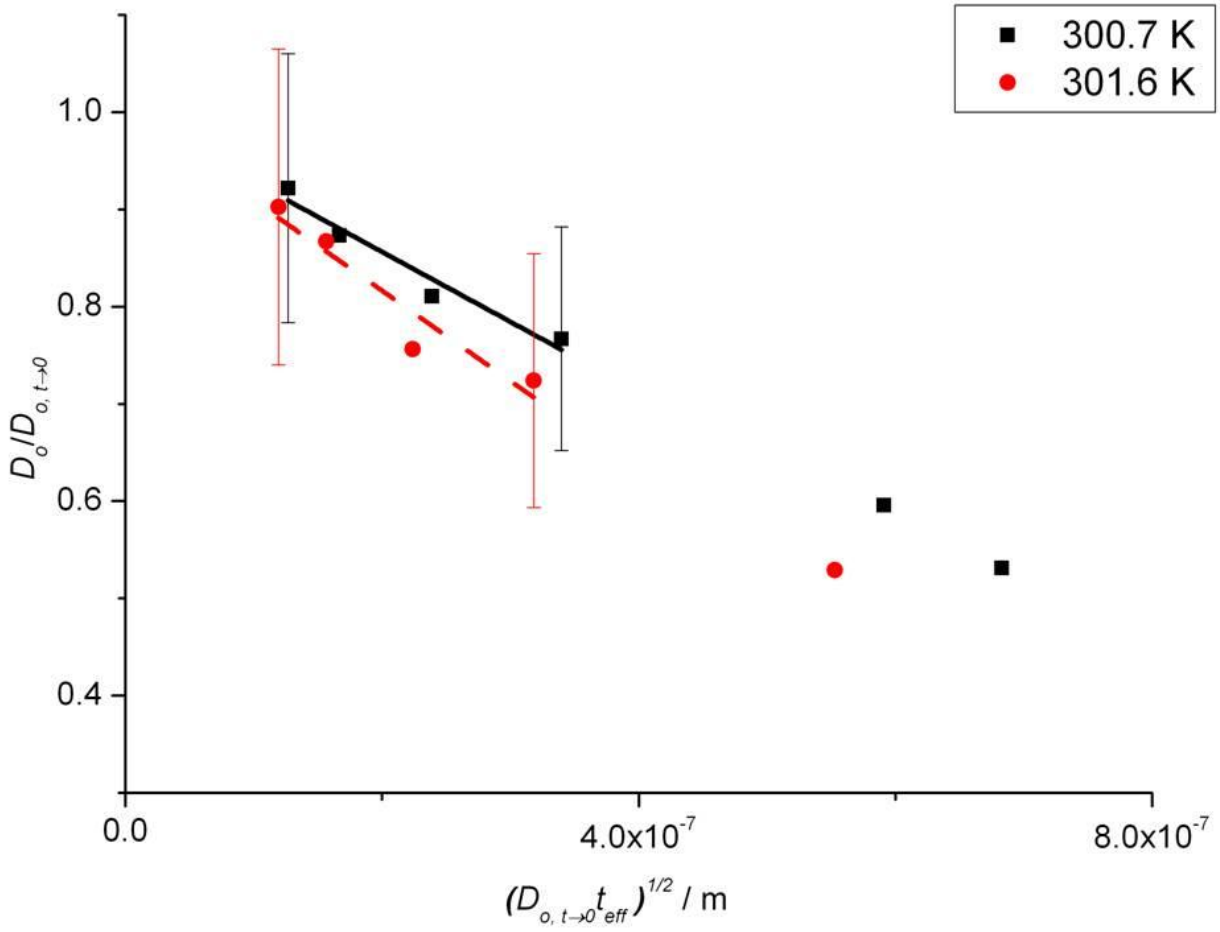

Figure 3-8. The ratio of the time-dependent effective diffusion coefficient of lipids in liquid-ordered domains relative to completely unrestricted diffusion in those domains as a function of $\left(D_{0,t\to 0}t_{eff}\right)^{1/2}$. Fitting of the data at short effective diffusion times by Equation 19 gives the surface-to-volume ratio of the domains.

the volume of the domain, is of the same order as the deviation of the propagator from that of Gaussian propagator describing unrestricted diffusion.[120] For the ensemble of molecules that started their trajectories inside the domains and did not attempt to diffuse through the domain boundaries by the time *t,* the ratio of the effective diffusion coefficient at time *t* and $D_{o,t\to 0}$ is given by the short-time limit by Mitra et al.[120]

$$\frac{D_o}{D_{o,t\to 0}} = 1 - \frac{4}{3d\sqrt{\pi}} \frac{(D_0 t)^{1/2} S}{V_p} + O(D_0 t) \qquad (19)$$

where D_o is the time-dependent diffusivity of molecules in the domain and *d* is the dimensionality of the space where diffusion takes place. For the considered lateral diffusion in lipid bilayers, *d* = 2. The experimental values for $D_{o,t\to 0}$ were obtained from a linear extrapolation of D_o vs. $\sqrt{t}$ (not shown) to *t* = 0. Such type of extrapolation is frequently used to determine diffusivity in the limiting case of small diffusion times.[52,53] For applications of Eq. 19 to time-dependent diffusion behavior of lipids in liquid-ordered domains, the higher order terms are considered to be negligible and the S/V_p ratio is taken as the ratio of the surface perimeter to the surface area. Figure 3-8 shows the plot of the ratio of D_o to $D_{o,t\to 0}$ as a function of $\left(D_{o,t\to 0} t_{eff}\right)^{1/2}$ for the two temperatures nearest to the transition temperature where T_1 NMR relaxation times are minimal, 300.7 and 301.6 K. For each temperature, initial data points were fitted by Equation 19 to obtain S/V_p. Data corresponding to higher effective diffusion times were excluded from the fit to hold the short-time limit requirement. For these calculations it was assumed that the liquid-ordered domains were circular in shape and there was no distribution of domain size over the bilayer. Table 3-2 gives the radius at each temperature and the

associated uncertainty. Because only initial data points were used for the fit, the uncertainty associated with relatively large using this method.

Table 3-2. The characteristic domain sizes as calculated by the fit of data in Figure 3-8 by Equation 19.

	300.7 K	**301.6 K**
R_{lo}, nm	523 ± 330	406 ± 250

Once significant concern associated with this method is related to the observation that Eq. 19 was derived for molecules that never left the original l_o domain by a given time *t.* At the same time, the corresponding ensemble of molecules considered in the experiment also includes molecules that left the domains but returned back to the same domain at the time *t* (in addition to the molecules that never left the domain). Another significant concern is associated with the assumption used to derive Eq. 19, *i.e.*, namely the absence of transport barriers at the domain boundaries. The discussion in the next section demonstrates that comparison of the PFG NMR data with the corresponding results of dynamic Monte Carlo simulation provides a better approach to get information on the domain sizes and the permeabilities of the domain boundaries.

Dynamic Monte Carlo Simulations

Complementary dynamic Monte Carlo (MC) simulations of molecular diffusion on square lattice were performed to extract information on the permeability of the domain boundaries and domain sizes from the measured PFG NMR data. Such simulations as well as the procedure of fitting PFG NMR results by the corresponding results of simulations to estimate permeabilities and domain sizes were recently reported in several papers.[122-125] Collaborative dynamic Monte Carlo simulations were performed by fellow graduate and undergraduate students, Amrish Menjoge and Robert Mueller, working in the research group of Sergey Vasenkov at the University of Florida. Briefly,

in complete analogy with the lattice described in reference 122, the two-dimensional simulation lattice used in this work consists of four square domains representing domains of liquid-ordered phase (l_o) that are surround by the inter-domain lattice representing the liquid-disordered (l_d) phase (Figure 3-9). The fractions of the lattice area occupied by the l_o and l_d phases in the simulation lattice were chosen to approximately correspond to those of the respective lipid fractions obtained from PFG NMR diffusion measurements in Table 3-1. The size of the simulation lattice shown in Fig. 3-9 was $L \times L$ ($L = 262 \times l$, where l is the length of the elementary diffusion step) and the size of the l_o domains was $L_o \times L_o$ ($L_o = 92 \times l$). Lipid diffusion was simulated by random walk on this lattice. Periodic boundary conditions were applied at the lattice boundaries. The probability of an elementary diffusion step inside the l_o domain in the x- or y- direction is denoted as p_{lo} and that through the domain boundary leading into the l_d phase is denoted as p_{blo} ($1 \le p_{lo}/p_{blo} \le 1{,}000$). The corresponding probability of an elementary diffusion step inside the l_d phase in the x- or y- direction is denoted as p_{ld} and that through the domain boundary leading into the l_o is denoted as p_{bld}. The experimentally observed difference between diffusivities in the l_o and l_d phases was taken into account by choosing $p_{ld}/p_{lo} = 2$ resulting in $p_{bld}/p_{blo} = 2$. The starting points of 10,000 random walkers were randomly selected on the lattice. The N-step walks ($N \le$ 10,000) were then generated for each random walker. The final simulations results reported here were the averages over 3 lattices with different configurations of the starting points. The quantities recorded in the simulations were the relative number of labeled random walkers, *i.e.*, those that were inside an l_o domain at time $t = 0$ and were

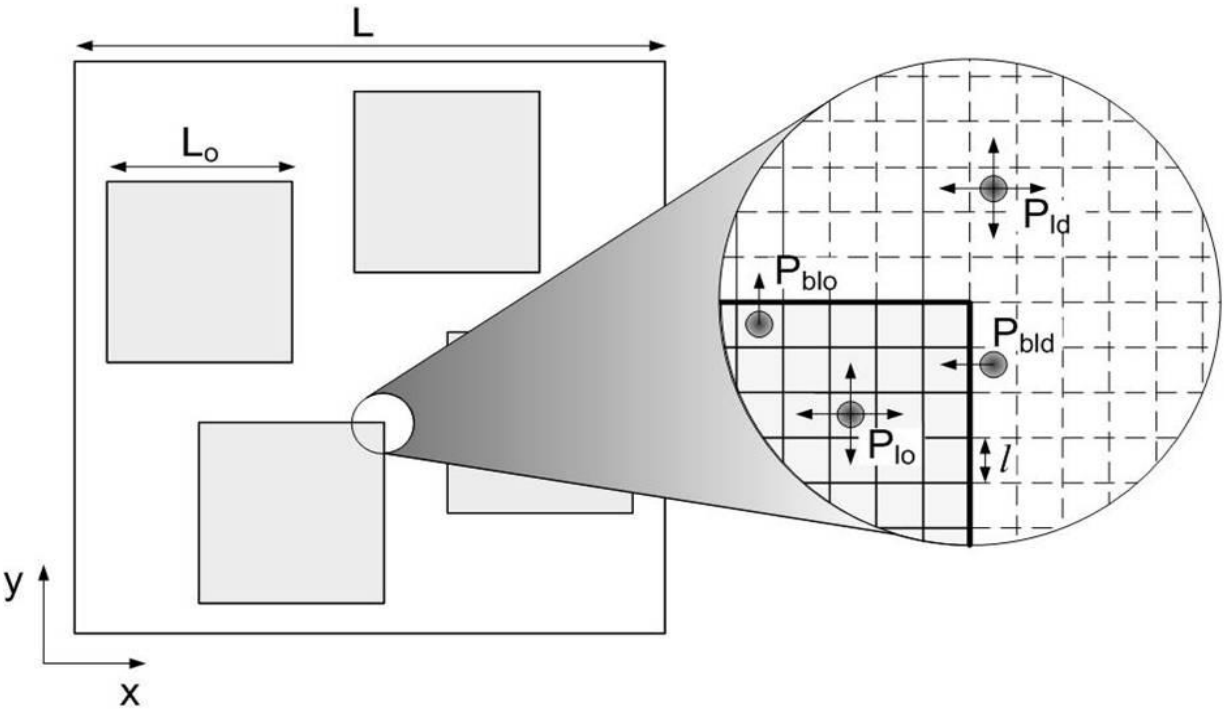

Figure 3-9. Two-dimensional simulation model for lipid bilayer. The periodic structure is organized by repetition of the simulation lattice of length L. The square domains of length L_o represent the liquid-ordered phase (l_o), and the surrounding inter-domain latticed represents the liquid-disordered phase (l_d). The inset shows various jump probabilities and the elementary diffusion step used in the simulation model.[126]

still inside the same domain at a later time t, ($N(t)/N_0$, where $N_0 = N(t=0)$), as well as normalized effective diffusivity of these random walkers, $D_o/D_{o,t\to 0}$, where $D_{o,t\to 0}$ is the diffusivity inside l_o domains at sufficiently small time when the domain boundaries do not influence diffusion behavior. The diffusion time is definite as $t = N\times\tau$, where τ is the duration of the elementary diffusion step. The effective diffusivity D_o is calculated from the Einstein equation Eq. 5. Based on the formulism discussed in Ref. 122, the probability p_{blo} can be used for calculation of the permeability of the domain boundaries for molecules (α) as

$$\alpha = p_{bl_o}\frac{D_{o,t\to 0}}{l} \tag{20}$$

Varying p_{blo} is thus equivalent to varying α in our simulations.

Figure 3-10 shows the results of fitting experimental data for T = 300.7 K with the corresponding results of the dynamic Monte Carlo simulations outlined above. Such fitting procedure was recently introduced to determine surface permeability of nanoporous particles.[125] Fig. 3-10 plots the ratio of the effective diffusivity of lipid molecules residing in l_o domains (D_o) to the $D_{o,t\to 0}$, as a function of diffusion time. The simulated curves were obtained for the values of the permeability of domain boundary, α, corresponding to a range between the limiting case when the domain boundary provides no transport barriers for lipid molecules (α = 1.1×10^{-3} m/s in Fig. 3-9), and a values of α which is almost two orders of magnitude smaller (α = 2.0×10^{-5} m/s in Fig. 3-9). Fig. 3-9A indicates that there is only an insignificant difference between the simulation results for different barrier permeabilities used. These differences are especially small for values of the ratio $D_o/D_{o,t\to 0}$ close to 1. Fitting the initial experimental data points (*i.e.*, those at small times when α does not affect D_o) to the simulated curves in Fig. 3-10A was used to determine the correlation between the experimental diffusion time and the diffusion time used in the simulation. The corresponding correlation between the length scales in the experiment and simulation was obtained by comparing the absolute values of diffusivities at a fixed time. Fig. 3-10B shows a plot of the relative number of molecules γ^* which at initial time (t = 0) have started their trajectories inside l_o domains and were outside these domains by the time shown on the horizontal axis of the figure. Such dependencies are often referred to as tracer exchange curves. Since the relationship between the diffusion time in the experiment and simulation was already determined in Fig. 3-10A, there are no “free”

parameters that can be used to adjust the correspondence between the experimental and simulation data in Fig. 3-10B. In contrast to the data in Fig. 3-10A, there is a significant difference between the simulation data for different values of α in Fig. 3-10B. It is seen in Fig. 3-10B that within the experimental uncertainty, the experimental data agrees with the simulation results obtained for $\alpha \geq 5.0 \times 10^{-4}$ m/s. Hence, we estimate that the permeability of the l_o domain boundary to be equal to or greater than 5.0×10^{-4} m/s at 300.7 K. Using the relationship between the length scales in the experiment and simulations as well as the domain size used in the simulations, we estimate the domain radius (R_{lo}) to be 930 ± 290 nm at 300.7 K. These estimates for α and R_{lo} were obtained assuming that all domains are circular and there is no distribution over domain sizes as well as over permeabilities of the domain boundaries and intra-domain diffusivities. The size of the square domains used in simulations was used to determine the radius of the corresponding circular domains by equating the perimeter-to-area ratios for both domain shapes. Similar treatment of the experimental data recorded at 301.6 K resulted in $\alpha \geq 9.2 \times 10^{-4}$ m/s and R_{lo} = 730 ± 310 nm (Table 3-3). Uncertainties associated with the domain radius using this method were smaller in comparison to the previous Mitra formulism as fits were obtained using all data points instead of those obtained at short times.

Table 3-3. Domain Properties at Temperatures Near T_m

	300.7 K	**301.6 K**
α, m/s	$\geq 5.0 \times 10^{-4}$	$\geq 9.2 \times 10^{-4}$
R_{lo}, nm	930 ± 290	730 ± 310

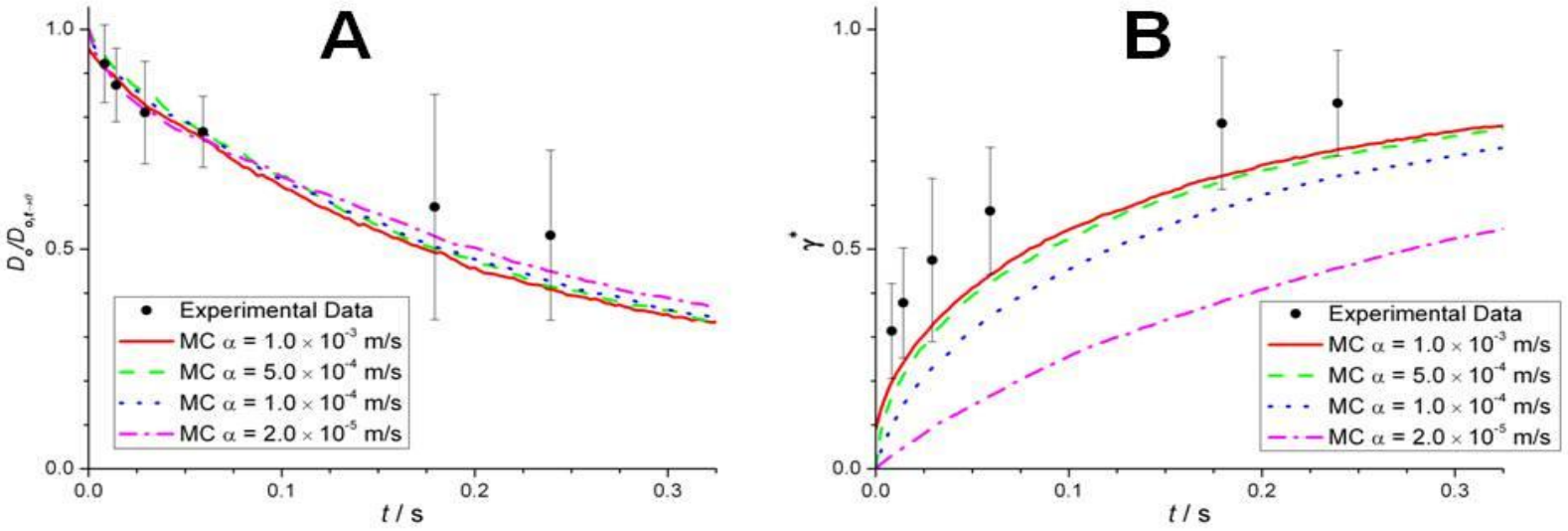

Figure 3-10. Examples of fitting experimental data (points) by the results of dynamic Monte Carlo (MC) simulations (lines). The data is fit for the following two dependencies: (A) time dependence of the ratio of the effective diffusivity of molecules in the liquid-ordered domains to the corresponding unrestricted diffusivity in these domains (*i.e.*, the diffusivity for the limiting case of small times) and (B) time dependence of the normalized fraction of molecules (γ^*) that started their trajectory inside the domains but ended their trajectory outside of domains. Experimental data was obtained at 300.7 K. The results of MC simulations are shown for different permeability of the domain boundaries (α).

PFG NMR at high-field and high-gradient strength was used to directly monitor the exchange of lipids between l_o and l_d phases that coexist in ternary lipid bilayers. This experimental option provides the possibility to monitor diffusion over length scales which are comparable to the size of l_o domains in membranes. Exchange was observed to occur over the time scales of the experimental diffusion times and was found to become more pronounced as the bilayers temperature was increased towards the miscibility transition temperature. The latter can be explained by an increase in diffusivity and some decrease in the characteristic domain sizes with an increase in temperature. Comparison of the experimental data and the corresponding results of dynamic Monte Carlo simulations allowed for the estimation of domain boundary permeability and domain size at temperatures near the transition temperature. The observed size of domains is still quite large in comparison to the minimum displacement that can be observed with the proposed experimental setup. It is then quite possible and would be very interesting to use this technique to study the exchange of lipids between domains in systems that form even smaller, biologically relevant l_o domains.

CHAPTER 4
SIGNIFICANCE AND FUTURE DIRECTIONS

The observation and analysis of lipid exchange between the liquid-ordered domains and the surrounding liquid-disordered phases of model lipid bilayers creates a new direction for studies aiming to understand the roles of lipid rafts in eukaryotic cell membrane. Characterizing the dynamics of lipids in the presence of domains is especially important when one considers the relationship between lipids diffusing inside domains with the transport of other domain-associated molecules. The application of high-field, high-gradient pulsed field gradient NMR allowed for the possibility to measure lateral diffusion over a broad range of mean square displacements, including displacements much smaller than those that previously were technically possible to record in model membranes using similar techniques. The application of PFG NMR with high gradient strengths to observe lipid dynamics in multibilayer stacks required a significant amount of attention to development. This work shows that it is not only feasible to perform diffusion studies of lipids in bilayers with high-field, high-gradient PFG NMR but also to monitor lipid exchange between different membrane domains. Here, time-dependent diffusion behavior was used to extract information about the characteristic permeability of the domain boundaries. The latter property was obtained experimentally for the first time for any types of lipid membranes. The technique developed and used in this work can be used to perform time-dependent studies over much smaller length scales. Composition and temperature are two major factors that influence the size of liquid-ordered domains. These factors can be modified to change the characteristic domain size in the membrane. High-field, high-gradient PFG NMR can then be used to further study lipid exchange in smaller domains.

This experimental technique can also be adapted to more advanced studies of model lipid membranes containing membrane proteins and/or peptides. Influence of reconstitution of domain-associated peptides into lipid bilayers on lateral transport in these bilayers can be studied using PFG NMR at high-field, and high gradient strengths. Lipid bilayers reconstituted on solid supports haven also been used to investigate electrical properties, enzymatic reactions, and pathogen attack. The technique developed in this work can be utilized for applications which served to characterize the effects of any one of these biological processes on the dynamics of membrane-associated molecules. The advantages of a non-invasion experimental technique capable of extracting information about lateral diffusion over a broad range of diffusion times with superior spatial and temporal resolution would serve to benefit investigations of how these processes influence the translational dynamics of membrane molecules as well as the local structure of the membrane. Model lipid bilayers reconstituted on planar supports as wells as on the pore walls of nanoporous and mesoporous membranes offer biomimetic environments for the study of molecular dynamics of the membrane constituents. This work shows that PFG NMR with high-field, high-gradient can be adapted for diffusion studies in planar membranes to give new details about lipid dynamics and membrane structural properties. It also demonstrates the potential of the technique to observe dynamics in other types of model membrane as well as the influence of certain membrane-associated molecules and/or biological processes.

The last consideration for future work using PFG NMR with high-field and high gradient strengths is the potential applications for studies of live cells, *in vivo*. While one of the main advantages of NMR is that there is no requirement for bulky labels (*i.e.*

dyes) which have been found to disturb the membrane, labels in the form of certain NMR-sensitive isotopes such as ^{13}C and ^{19}F can be incorporated into membrane molecules and utilized in a non-invasive manner. Observation of diffusion of such labeled molecules in vivo using PFG NMR with high-field and high gradient strengths can be feasible.

LIST OF REFERENCES

(1) Singer, S. J.; Nicolson, G. L. *Science* **1972**, *175*, 720.

(2) Simons, K.; Toomre, D. *Nat. Rev. Mol. Cell. Biol.* **2000**, *1*, 31.

(3) Pike, L. J. *J. Lipid Res.* **2009**, *50*, S323.

(4) Simons, K.; Ikonen, E. *Nature* **1997**, *387*, 569.

(5) Simons, K.; van Meer, G. *Biochemistry* **1988**, *27*, 6197.

(6) Fantini, J.; Garmy, N.; Mahfoud, R.; Yahi, N. *Expert Rev. Molec. Medicine* **2002**, *20*, 1.

(7) Wielgosz, M. M.; Rauch, D. A.; Jones, K. S.; Ruscetti, F. W.; Ratner, L. *AIDS Res Hum Retroviruses* **2005**, *21*, 43.

(8) Aloia, R. C.; Tian, H.; Jensen, F. C. *Proc. Natl. Acad. Sci. U S A* **1993**, *90*, 5181.

(9) Hill, J. M.; Steiner, I.; Matthews, K. E.; Trahan, S. G.; Foster, T. P.; Ball, M. J. *Med Hypotheses* **2005**, *64*, 53.

(10) Freeman, M. R.; Solomon, K. R. *J. Cell Biochem* **2004**, *91*, 54.

(11) Zhuang, L. Y.; Kim, J.; Adam, R. M.; Solomon, K. R.; Freeman, M. R. *J. Clin Invest* **2005**, *115*, 959.

(12) Zaremberg, V.; Gajate, C.; Cacharro, L. M.; Mollinedo, F.; McMaster, C. R. *J. Biol. Chem.* **2005**, *280*, 38047.

(13) Brown, D. A.; London, E. *Annu. Rev. Cell Dev. Biol.* **1998**, *14*, 111.

(14) Reitveld, A.; Simons, K. *Biochim. Biophys. Acta.* **1998**, *1376*, 467.

(15) Sankaram, M. B.; Thompson, T. E. *Biochemistry* **1990**, *29*, 10670.

(16) Bagatolli, L. A.; Gratton, E. *Biophys. J.* **2000**, *78*, 290.

(17) Ahmed, S. N.; Brown, D. A.; London, E. *Biochemistry* **1997**, *36*, 10944.

(18) Dietrich, C.; Bagatolli, L. A.; Volvyk, Z. N.; Thompson, N. L.; Levi, M.; Jacobson, K.; Gratton, E. *Biophys. J.* **2001**, *80*, 1417.

(19) Korlach, J.; Schwille, P.; Webb, W. W.; Feigenson, G. *Proc. Natl. Acad. Sci. USA* **1999**, *96*, 8461.

(20) Mukherjee, S.; Maxfield, F. R. *Annu. Rev. Cell Dev. Biol. 2004. 20:839–66* **2004**, *20*, 839.

(21) Mayor, S.; Rao, M. *Traffic* **2004**, *5*, 231.

(22) Binder, W. H.; Barragan, V.; Menger, F. M. *Angew. Chem. Int. Ed.* **2003**, *42*, 5802

(23) McConnell, H. M.; Vrljic, M. *Annu. Rev. Biophys. Biomol. Struct.* **2003**, *32*, 469.

(24) Silvius, J.; Nabi, I. R. *Molec. Membrane Biol.* **2006**, *23*, 5.

(25) de Almeida, R. F. M.; Loura, L. S.; Fedorov, A.; Prieto, M. *J. Mol. Biol.* **2005**, *346*, 1109.

(26) Silvius, J. R. *Biophys. J.* **2003**, *85*, 1034.

(27) Loura, L. S.; Fedorov, A.; Prieto, M. *Biophys. J.* **2001**, *80*, 776.

(28) de Almeida, R. F. M.; Fedorov, A.; Prieto, M. *Biophys. J.* **2003**, *85*, 2406.

(29) Veatch, S. L.; Keller, S. L. *Biophys. J.* **2003**, *85*, 3074.

(30) Feigenson, G. W.; Buboltz, J. T. *Biophys. J.* **2001**, *80*, 2775.

(31) Kahya, N.; Scherfeld, D.; Bacia, K.; Poolman, B.; Schwille, P. *J. Biol. Chem.* **2003**, *78*, 28109.

(32) Dietrich, C.; Volovyk, Z. N.; Levi, M.; Thompson, N. L.; Jacobson, K. *PNAS* **2001**, *98*, 10642.

(33) Wang, T.-Y.; Silvius, J. R. *Biophys. J.* **2003**, *84*, 367.

(34) Yuan, C.; Furlong, J.; Burgos, P.; Johnston, L. J. *Biophys. J.* **2002**, *82*, 2526.

(35) Rinia, H. A.; Snel, M. M. E.; van der Eerden, J. P. J. M.; de Kruijff, B. *FEBS Letters* **2001**, *501*, 92.

(36) Tokumasu, F.; Jin, A. J.; Feigenson, G. W.; Dvorak, J. A. *Biophys. J.* **2003**, *84*, 2609.

(37) Dufrêne, Y. F.; Lee, G. U. *Biochim. Biophys. Acta.* **2000**, *1509*, 14.

(38) Melchior, D. L. *Science* **1986**, *234*, 1577.

(39) Epand, R. M. *Biophysical Chemistry* **2007**, *126*, 197.

(40) McMullen, T. P. W.; McElhaney, R. N. *Biochim. Biophys. Acta.* **1995**, *1234*, 90.

(41) Sankaram, M. B.; Marsh, D.; Gierasch, L. M.; Thompson, T. E. *Biophys. J.* **1994**, *66*, 1959.

(42) Collado, M. I.; Goni, F. M.; Alonso, A.; Marsh, D. *Biochemistry* **2005**, *44*, 4911.

(43) Veatch, S. L.; Polozov, I. V.; Gawrisch, K.; Keller, S. L. *Biophys. J.* **2004**, *86*, 2910.

(44) Aussenac, F.; Tavares, M.; Dufourc, E. J. *Biochemistry* **2003**, *42*, 1383.

(45) Holland, G. P.; McIntyre, S. K.; Alam, T. M. *Biophys. J.* **2006**, *90*, 4248.

(46) Polozov, I. V.; Gawrisch, K. *Biophys. J.* **2006**, *90*, 2051.

(47) *Lipid Rafts and Cavaolae: From Membrane Biophysics to Cell Biology*; Fielding, C. J., Ed.; Wiley-VCH: Weinheim, 2006.

(48) Brown, D. A.; Rose, J. K. *Cell* **1992**, *68*, 533.

(49) Lommerse, P. H. M.; Spaink, H. P.; Schmidt, T. *Biochim. Biophys. Acta.* **2004**, *1664*, 119.

(50) Kenworthy, A. K.; Nichols, B. J.; Remmert, C. L.; Hendrix, G. M.; Kumar, M.; Zimmerberg, J.; Lippincott-Schwartz, J. *J. Cell Biology* **2004**, *165*, 735.

(51) McMullen, T. P. W.; Lewis, R. N. A. H.; McElhaney, R. N. *Curr. Opin. Colloid In.* **2004**, *8*, 459.

(52) Kusumi, A.; Ike, H.; Nakada, C.; Murase, K.; Fujiwara, T. *Semin. Immunol.* **2005**, *17*, 3.

(53) Munro, S. *Cell* **2003**, *115*, 377.

(54) Glebov, O.; Nichols, B. J. *Nat. Cell Biol.* **2004**, *6*, 238.

(55) Nichols, B. *Nature* **2005**, *436*, 638.

(56) Lenne, P.-F.; Nicolas, A. *Soft Matter* **2009**, *5*.

(57) Brugger, B.; Glass, B.; Haberkant, P.; Leibrecht, I.; Wieland, F. T.; Krausslich, H.-G. *PNAS* **2006**, *103*, 2641.

(58) Meder, D.; Moreno, M. J.; Verkade, P.; Vaz, W. L. C.; Simons, K. *PNAS* **2006**, *103*, 329.

(59) Swamy, M. J.; Ciani, L.; Ge, M.; Smith, A. K.; Holowka, D.; Baird, B.; Freed, J. H. *Biophys. J.* **2006**, *90*, 4452.

(60) Sengupta, P.; Baird, B.; Holowka, D. *Semin. Cell Dev. Biol.* **2007**, *18*, 583.

(61) Eggeling, C.; Ringemann, C.; Medda, R.; Schwarzmann, G.; Sandhoff, K.; Polyakova, S.; Belov, V. N.; Hein, B.; von Middendorff, C.; Schonle, A.; Hell, S. W. *Nature* **2009**, *457*, 1159.

(62) Fabien, P.; Xavier, M.; Gopal, I.; Emmanuel, M.; Hsiao-Ping, M.; Shimon, W. *Traffic* **2009**, *10*, 691.

(63) Oelke, J.; Pasc, A.; Wixforth, A.; Konovalov, O.; Tanaka, M. *Appl. Phys. Lett.* **2008**, *93*, 213901.

(64) Anderson, R. G. W.; Jacobson, K. *Science* **2002**, *296*, 1821.

(65) Jacobson, K.; Mouritsen, O. G.; Anderson, R. G. W. *Nat Cell Biol* **2007**, *9*, 7.

(66) Janes, P. W.; Ley, S. C.; Magee, A. I. *J. Cell Biol.* **1999**, *147*, 447.

(67) Dykstra, M.; Cherukuri, A.; Sohn, H. W.; Tzeng, S. J.; Pierce, S. K. *Annu. Rev. Immunol.* **2003**, *21*, 457.

(68) Johnston, L. J. *Langmuir* **2007**, *23*, 5886.

(69) Veatch, S. L.; Soubias, O.; Keller, S. L.; Gawrisch, K. *Proc. Nat. Acad. Sci.* **2007**, *104*, 17650.

(70) Radhakrishnan, A.; McConnell, H. *J. Chem. Phys.* **2007**, *126*, 185101.

(71) Nielsen, L. K.; Bjornholm, T.; Mouritsen, O. G. *Nature* **2000**, *404*, 352.

(72) Gomez, J.; Sagues, F.; Reigada, R. *Phys. Rev. E* **2008**, *77*, 021907.

(73) Pandit, S. A.; Jakobsson, E.; Scott, H. L. *Biophys. J.* **2004**, *87*, 3312.

(74) Garbès Putzel, G.; Schick, M. *Biophys. J.* **2008**, *94*, 869.

(75) Shaw, J. E.; Epand, R. F.; Epand, R. M.; Li, Z.; Bittman, R.; Yip, C. M. *Biophys. J.* **2006**, *90*, 2170.

(76) Samiee, K. T.; Moran-Mirabal, J. M.; Cheung, Y. K.; Craighead, H. G. *Biophys. J.* **2006**, *90*, 3288.

(77) Edel, J. B.; Wu, M.; Baird, B.; Craighead, H. G. *BBA - Biomembranes* **2005**, *1668*, 158.

(78) Saffman, P. G.; Delbruck, M. *Proc. Nat. Acad. Sci. U.S.A.* **1975**, *72*, 3111.

(79) Price, W. S. *Concepts Magn. Reson.* **1998**, *10*, 197.

(80) Wu, E.; Jacobson, K.; Papahadjopoulos, D. *Biochemistry* **2002**, *16*, 3936.

(81) Mullineaux, C.; Kirchhoff, H. Using Fluorescence Recovery After Photobleaching to Measure Lipid Diffusion in Membranes. In *Methods in Membrane Lipids*; Dopico, A., Ed.; Humana Press, 2007; Vol. 400.

(82) Okazaki, T.; Inaba, T.; Tatsu, Y.; Tero, R.; Urisu, T.; Morigaki, K. *Langmuir* **2008**, *25*, 345.

(83) Schwille, P.; Korlach, J.; Webb, W. W. *Cytometry* **1999**, *36*, 176.

(84) Saxton, M. J. *Biophys. J.* **1997**, *72*, 1744.

(85) Selle, C.; Ruckerl, F.; Martin, D. S.; Forstner, M. B.; Kas, J. A. *Phys. Chem. Chem. Phys.* **2004**, *6*, 5535.

(86) Dietrich, C.; Yang, B.; Fujiwara, T.; Kusumi, A.; Jacobson, K. *Biophys. J.* **2002**, *82*, 274.

(87) Scheidt, H. A.; Huster, D.; Gawrisch, K. *Biophys. J.* **2005**, *89*, 2504.

(88) Orädd, G.; Westerman, P. W.; Lindblom, G. *Biophys. J.* **2005**, *89*, 315.

(89) Lindblom, G.; Orädd, G.; Filippov, A. *Chem. Phys. Lipids* **2006**, *141*, 179.

(90) Filippov, A.; Orädd, G.; Lindblom, G. *Biophys. J.* **2004**, *86*, 891.

(91) Orädd, G.; Lindblom, G. *Magn. Reson. Chem.* **2004**, *42*, 123.

(92) Hahn, E. L. *Phys. Rev.* **1950**, *80*, 580.

(93) Stallmach, F.; Galvosas, P. *Annu. Rep. NMR Spectrosc.* **2007**, *61*.

(94) Tanner, J. E. *J. Chem. Phys.* **1970**, *52*, 2523.

(95) Levitt, M. H. *Spin Dynamics: Basics of Nuclear Magnetic Resonance*; John Wiley & Sons, LTD.: New York, 2001.

(96) Vasenkov, S.; Galvosas, P.; Geier, O.; Nestle, N.; Stallmach, F.; Kärger, J. *J. Magn. Reson.* **2001**, *149*, 228.

(97) Galvosas, P.; Stallmach, F.; Seiffert, G.; Kärger, J.; Kaess, U.; Majer, G. *J. Magn. Reson.* **2001**, *151*, 260.

(98) Cotts, R. M.; Hoch, M. J. R.; Sun, T.; Markert, J. T. *J. Magn. Reson.* **1989**, *83*, 252.

(99) Kärger, J.; Ruthven, D. M. *Diffusion in Zeolites and Other Microporous Solids*; Wiley & Sons: New York, 1992.

(100) Boxer, S. G. *Curr. Opin. Chem. Biol.* **2000**, *4*, 704.

(101) Sackmann, E. *Science* **1996**, *271*, 43.

(102) Kalb, E.; Frey, S.; Tamm, L. K. *Biochim. Biophys. Acta.* **1992**, *1103*, 307.

(103) Nollert, P.; Kiefer, H.; Jähnig, F. *Biophys. J.* **1995**, *69*, 1447.

(104) Kuo, A.-L.; Wade, C. G. *Biochemistry* **2002**, *18*, 2300.

(105) Hallock, K. J.; Henzler Wildman, K.; Lee, D.-K.; Ramamoorthy, A. *Biophys. J.* **2002**, *82*, 2499.

(106) Gaede, H. C.; Luckett, K. M.; Polozov, I. V.; Gawrisch, K. *Langmuir* **2004**, *20*, 7711.

(107) Lindblom, G.; Orädd, G. *J. Disp. Sci. Technol.* **2007**, *28*, 55.

(108) Pampel, A.; Zick, K.; Glauner, H.; Engelke, F. *J. Am. Chem. Soc.* **2004**, *126*, 9534.

(109) Polozov, I. V.; Gawrisch, K. *Biophys. J.* **2004**, *87*, 1741.

(110) Dvinskikh, S. V.; Furo, I. *J. Magn. Reson.* **2000**, *144*, 142.

(111) Sorland, G. H.; Dagfinn, A. *Magn. Reson. Chem.* **2002**, *40*, S139.

(112) Mitra, P.; Halperin, B. *J. Magn. Reson. A* **1995**, *113*, 94.

(113) Malmborg, C.; Topgaard, D.; Soderman, O. *J. Magn. Reson.* **2004**, *169*, 85.

(114) Gibbs, S. J.; Johnson, C. S. *J. Magn. Reson.* **1991**, *93*, 395.

(115) Orädd, G.; Lindblom, G. *Spect. Int. J.* **2005**, *19*, 191.

(116) Lindblom, G.; Orädd, G. *Biochim. Biophys. Acta.* **2009**, *1788*, 234.

(117) Kroon, P. A.; Kainosho, M.; Chan, S. I. *Nature* **1975**, *256*, 582.

(118) Deese, A. J.; Dratz, E. A.; Hymel, L.; Fleischer, S. *Biophys. J.* **1982**, *37*, 207.

(119) Mitra, P. P.; Sen, P. N.; Schwartz, L. M. *Phys. Rev. B* **1993**, *47*, 8565.

(120) Mitra, P. P.; Sen, P. N.; Schwartz, L. M.; Le Doussal, P. *Phys. Rev. Lett.* **1992**, *68*, 3555.

(121) Latour, L. L.; Mitra, P. P.; Kleinberg, R. L.; Sotak, C. H. *J. Magn. Reson. A* **1993**, *101*, 342.

(122) Krutyeva, M.; Kärger, J. *Langmuir* **2008**, *24*, 10474.

(123) Krutyeva, M.; Vasenkov, S.; Kärger, J. *Magn. Reson. Imag.* **2007**, *25*, 567.

(124) Krutyeva, M.; Vasenkov, S.; Yang, X.; Caro, J.; Kärger, J. *Microporous Mesoporous Mat.* **2007**, *104*, 89.

(125) Krutyeva, M.; Yang, X.; Vasenkov, S.; Kärger, J. *J. Magn. Reson.* **2007**, *185*, 300.

(126) Sanders, M.; Mueller, R.; Menjoge, A.; Vasenkov, S. *J. Phys. Chem. B* **2009**, *113*, 14355.

BIOGRAPHICAL SKETCH

Monica Danielle Sanders was born in Lubbock, Texas to James Kirk Sanders and Cynthia Sanders Buettner. She grew up in Moore, Oklahoma with her mother, stepfather, Rick Buettner, and younger brother, Kevin Buettner. She graduated from Moore High School in 2000 with valedictorian honors. She earned her B.S. in chemical engineering (biotechnology) and her minor in Spanish from the University of Oklahoma (OU) in 2005. Upon receiving her B.S., she attended graduate school at the University of Florida (UF), where she obtained her Doctorate in chemical engineering.